J. Fluid Mech. (1984), *vol.* 148, *pp.* 349–382
Printed in Great Britain

Mixing and combustion with low heat release in a turbulent shear layer

By M. G. MUNGAL AND P. E. DIMOTAKIS
Graduate Aeronautical Laboratories, California Institute of Technology, Pasadena, CA 91125

(Received 19 September 1983 and in revised form 4 June 1984)

Turbulent mixing and combustion are investigated in a gaseous shear layer formed between two streams: one containing a low concentration of hydrogen in nitrogen and the other containing a low concentration of fluorine in nitrogen. The resulting temperature field is measured simultaneously at eight points across the width of the layer using fast-response cold-wire thermometry. The results show the presence of large, hot structures separated by tongues of cool fluid that enter the layer from either side. The usual bell-shaped mean-temperature profiles therefore result from a duty cycle whereby a fixed probe sees alternating hot and cool fluid, which results in the local mean. The adiabatic flame temperature is not achieved in the mean, at any location across the layer. For fixed velocities, it is found that, in general, two different mean-temperature profiles result from a given pair of reactant compositions if the sides of the layer on which they are carried are exchanged ('flipped'). This finding is a direct consequence of the asymmetric entrainment of fluid into the layer. Results are compared with the predictions of Konrad and discussed in the context of the Broadwell–Breidenthal model. By comparison with the liquid result of Breidenthal, the amount of product formed in the layer at high Reynolds number is found to be dependent upon the Schmidt number. Results for a helium–nitrogen layer are discussed briefly.

1. Introduction

Turbulent shear layers have been studied for several decades, and the discovery of large-scale structures in turbulent shear flows has greatly increased the experimental and theoretical activity in this area. More recently, mixing has been a phenomenon that has received considerable attention because of its importance to several technological areas, and to combustion in particular. This research should be viewed as a continuation of previous work performed at Caltech, such as that of Brown & Roshko (1971, 1974), Konrad (1976), Dimotakis & Brown (1976), Breidenthal (1978, 1981) and Bernal (1981), and also of the similar experiment of Wallace (1981) in Australia. The major difference between this investigation and the earlier work at Caltech is that the mixing layer is undergoing chemical reaction with heat release. It is anticiptated that the large-structure dynamics, which have already been shown to be quite important in the cold cases, will continue to be important when combustion takes place (Ganji & Sawyer 1980*a*,*b*; Wallace 1981; Pitz & Daily 1983; Keller & Daily 1983).

The experimental facility has been designed to be capable of maximum flame temperatures of 1000 K above ambient, but the present work is performed at low heat release with maximum flame temperatures of 165 K above ambient. The current

aim is to study mixing and product formation in the limit of low heat release to achieve a more basic understanding of these phenomena, and to provide part of the data base with which the results of subsequent experiments involving higher heat release can be compared. For the purposes of this work, low heat release is considered to be the regime for which the overall properties of the layer are not significantly changed from the cold case. Wallace (1981) has previously identified such flows to be those for which the maximum mean-temperature rise is less than 100 K above ambient, corresponding to an average density decrease of about 15 % within the layer.

The two-dimensional turbulent mixing layer is a relatively simple flow that is well documented and is encountered in many practical combustor designs. By adding to both streams low concentrations of various reactants that release heat spontaneously and rapidly, it is possible to study the amount of product formed in a simple flow from which problems of flameholders and igniters have been eliminated. It is possible to investigate, with low reactant concentrations, the effects of concentration ratio. With higher reactant concentrations, it is possible to investigate the effects of heat release upon the flow itself. The present experiment uses hydrogen and fluorine (together with trace amounts of nitric oxide, for rapid and uniform ignition) to achieve these ends – the reaction is simple, fast, highly exothermic and well documented. Thus this work should be viewed as an attempt to address the more general and difficult problem of turbulent mixing and combustion in a manner in which the fluid mechanics and chemical kinetics remain tractable. In fact, it is thought that, if any problem in turbulent combustion holds out hope for analytic or computational description, then surely this must be a prime candidate.

1.1. *Chemical-reaction method*

Breidenthal (1978, 1981) has pointed out that the amount of molecular scale mixing in a turbulent shear layer between two streams can be measured in at least two ways. The passive-scalar technique consists of introducing a passive scalar contaminant into one stream and measuring the local instantaneous concentration as a function of time. If the probe sampling volume is small compared to the smallest concentration scales then it is possible to measure the true local concentration and to infer the product formation at that point (Toor 1962). If, however, the sampling volume is too large, concentration fluctuations will be smoothed out and the inferred amount of mixing or chemical reaction will be overestimated.

The second technique is to use a method whereby the mixing at the molecular level is displayed macroscopically in some conveniently measurable fashion. Such a process is a fast second-order chemical reaction of the type $A + B \rightarrow P$. Thus, if dilute reactant A is added to one stream and dilute reactant B is added to the other, and if they react rapidly and irreversibly to form reaction product P, then the amount of product formed is directly proportional to the consumption of the lean reactant, and is a measure of the amount of molecular mixing. In contrast with the passive technique, a finite sampling volume does not inherently overestimate the amount of mixing. For the irreversible reaction the total amount of mixed fluid within the sampling volume is proportional to the amount of product there, independent of the size of the sampling volume.

Konrad (1976) used a concentration probe (see Brown & Rebollo 1972) to measure the mixing of a passive scalar. Breidenthal (1978, 1981) approximated the irreversible reaction with a reversible one using phenolphthalein and sodium hydroxide, i.e.

$$\text{phenolphthalein} + 2(\text{OH})^- \rightleftharpoons \text{red product}.$$

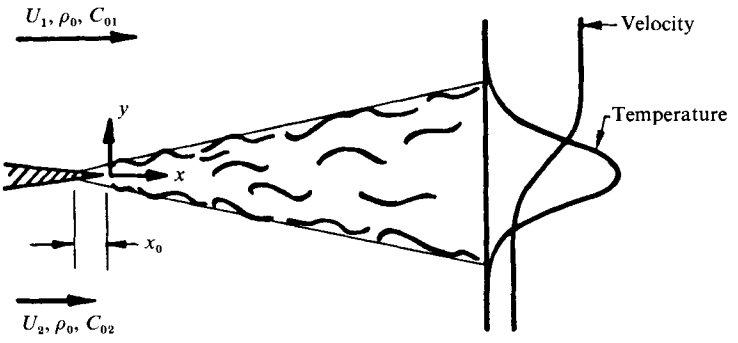

FIGURE 1. Turbulent shear-layer geometry.

which was probed by measuring the attenuation of a beam of green light. In the present investigation, the irreversible reaction is approximated to high accuracy by the reaction

$$H_2 + F_2 \rightarrow 2HF, \quad \Delta Q = -130\,\text{kcal mol}^{-1}.$$

This reaction is sufficiently energetic that 1 % F_2 and 1 % H_2 in nitrogen will produce an adiabatic flame temperature of 93 K above ambient (for this work, the adiabatic flame temperature is defined as the temperature rise attained if both reactants burn to completion, adiabatically, at constant pressure). Thus dilute concentrations produce significant temperature rises. As discussed later, the reaction actually consists of two second-order chain reactions with chemical times that are fast compared with the fluid-mechanical timescales.

It should also be stated that, while a long-term goal of the present studies is to investigate the effect of heat release on the mixing layer, the current results are entirely at the low-heat-release end of the spectrum where the heat itself serves to label the molecularly mixed fluid, so that, in this work, heat release (or temperature rise) and product formation are analogous.

The simple physical ideas contained in the Broadwell–Breidenthal model, together with their implications, guided the experiments, which were performed at a fixed Reynolds number, for a wide range of concentration ratios. Sections 2 and 3 give a description of the experimental facility and measuring techniques §§4–6 discuss the chemistry and theory involved, while §§7–11 present the results of the investigation together with some comparisons with other work. Some of the results described below have been presented briefly in Mungal, Dimotakis & Broadwell (1984); however, the emphasis here will be on the fluid-mechanical interpretation of these results.

2. Experimental apparatus

The reacting shear layer (figure 1) is produced in a new blowdown facility shown in figure 2. By using a partial-pressure technique, a given concentration of fluorine in nitrogen is loaded into a gastight FEP Teflon bag contained within the left reactant vessel (0.57 m^3 volume). A similar technique is used to load a charge of hydrogen in nitrogen into the right reactant tank. The outsides of the Teflon bags communicate with a much larger surge tank (12.7 m^3 volume), which provides the flow that is necessary to collapse the bags and displace the reactant charges while still maintaining an essentially constant upstream stagnation pressure. After the flow passes through

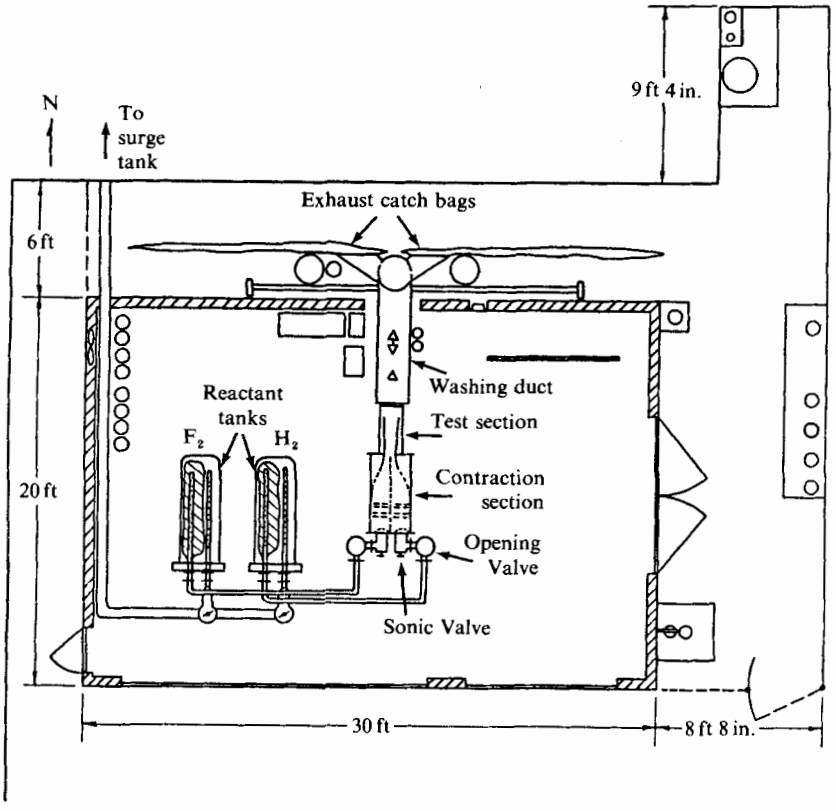

FIGURE 2. Layout of GALCIT reacting shear-flow laboratory.

the main opening valves, it is metered at a pair of sonic valves which remain choked during the course of a run.

The settling and contraction section is used to expand the flow from round to rectangular sections and contains 2 sets of perforated plate and 4 stations of fine-mesh screen (40 and 80 mesh) for turbulence reduction. The high-speed contraction ratio is 6:1 with an exit area of 5 cm × 20 cm, while the low-speed contraction ratio is 3:1 with an exit area of 10 cm × 20 cm. The high-speed contraction contour is defined by tangent circular arcs of 81 and 41 cm radii with the latter tangent to the test section. The length to inlet-height ratio of 2.5 meets the flow non-separation criterion suggested by Chmielewski (1974). In a similar fashion, the low-speed contraction contour is defined by a pair of tangent circular arcs of 102 and 43 cm radii. The splitter-tip included angle was less than 4°. The test section is 76 cm long, with the first 51 cm useful for flow measurements.

Once the hot toxic gas leaves the test section it enters a 51 cm diameter duct and is washed on the fly by a high-pressure sodium hydroxide atomized-spray system, which both cools the flow and partially neutralizes the hydrogen fluoride and unburnt fluorine. The exhaust gas is then captured in two large Teflon bags (11.3 m^3 total capacity) and is treated to remove remaining toxins at a later time.

3. Measurements

Runs were performed with flow velocities $U_1 = 22$ m/s and $U_2 = 8.8$ m/s for a speed ratio $r \equiv U_2/U_1 = 0.40$. The high-speed stream turbulence level was about $\frac{2}{3}$% r.m.s. All measurements were taken at the $x = 45.7$ cm station, where the visual width of the layer was about 7.4 cm. The Reynolds number based on velocity difference and visual thickness is 6.5×10^4, which is well past the mixing transition observed by Konrad (1976) in a gas and Breidenthal (1978, 1981) in a liquid. The high-speed boundary-layer momentum thickness θ_1 was estimated using Thwaites' method (White 1974), with the Reynolds number $U_1\theta_1/\nu$ estimated to be 240. Thus at the measuring station $x/\theta_1 \approx 2800$.

The equivalence ratio ϕ is defined here as the ratio of the low-speed free-stream reactant molar concentration c_{02} to the high-speed free-stream reactant molar concentration c_{01}, divided by the low-speed to high-speed stoichiometric ratio, i.e.

$$\phi = \frac{c_{02}/c_{01}}{(c_{02}/c_{01})_s} = \frac{c_{02}}{c_{01}},$$

since the molar stoichiometric ratio for the hydrogen–fluorine reaction is unity. Physically, the equivalence ratio, as defined, is the volume of high-speed fluid required to completely react with unit volume of low-speed fluid. This definition is appropriate here, as opposed to the conventional definition of the equivalence ratio (e.g. in diffusion-flame theory), where it is defined as the fuel-to-oxidizer ratio divided by the fuel-to-oxidizer stoichiometric ratio, i.e.

$$\phi = \frac{(f/o)}{(f/o)_s}$$

where f, o are normally taken to be mass fractions. As will be seen, for the purposes of this work there is no need to distinguish which species serves as the fuel and which as the oxidizer: the more important concern is the ratio of low-speed to high-speed reactant concentrations.

For each run, the streamwise pressure gradient is set to zero by adjustment of the low-speed sidewall. For all runs reported the low-speed velocity is estimated to be constant along the length of the test section to within 2%. The mean-velocity profile is measured by a rake of 15 Pitot tubes and recorded on a miniature manometer bank, which was photographed by a motor-driven 35 mm camera during each run. Temperature is recorded by a rake of 8 cold wires, placed across the width of the layer, each driven by a constant current, i.e. the wires are run as resistance thermometers. A simple preamplifier circuit provided 0.4 mA through each wire such that the output voltage was linearly proportional to the temperature rise. Each circuit was then followed by a additional gain stage and an 8 kHz low-pass filter. It is estimated that under conditions of natural convection (a worst case) the electrical heating causes a temperature rise of less than 0.2 K, which is negligible compared with the temperature rises of interest in the flow. The overall noise in the circuit also corresponded to about 0.2 K. A typical wire is made of 2.5 μm diameter 90% platinum – 10% rhodium welded to inconel prongs with a span of 1.5 mm yielding an aspect ratio of 600. The length of the wire divided by Betchov's (1948) 'cold length' is approximately 20 at the mean-flow conditions (see also Paranthoen, Petit & Lecordier 1982*a*). Each wire is sampled at 10 kHz during a run for a total data rate

of 80 kHz, which is recorded on a DEC LSI 11/23. It is observed experimentally that the response time of the probes varies from 330 μs on the high-speed side to 500 μs on the low-speed side (Paranthoen, Lecordier & Petit 1982*b*).

It should be noted that cold wires used for temperature measurement suffer from two main types of error (see Scadron & Warshawsky 1952; Paranthoen *et al.* 1982*b*). The first stems from the finite thermal mass of the wire and the associated response time, while the second results from the conduction of heat along the wire into the prong tips.

An important feature of the present measurements is the static calibration that was applied to each wire: prior to a run a small hot jet and a small cool jet (whose temperatures were accurately known) were applied to each probe in such a way that the entire wire and prong tips equilibrated to the jet temperature, and the probe voltages recorded. These two measurements thus provide the calibration constant to convert recorded voltage to temperature rise. During a run the reacting flow performs the same function as the hot jet; namely, it brings the prong tips to a local mean temperature about which the wire performs excursions. The mean temperature is therefore accurate to within the calibration procedure, to the extent that convective heat transfer to the wire is essentially the same from both hot and cool fluid regions. Excursions from the mean do, however, suffer from conduction error, which can be as high as 10–20 % for the wires used in these experiments.

The mean-temperature profiles shown below are quite repeatable from run to run; however, the absolute reactant concentrations are known only to within approximately 3–5 %, resulting in a corresponding uncertainty for the absolute value of heat release of the same order.

4. Chemical reactions

The chemical reaction utilized in this experiment consists of a pair of second-order chain reactions of differing rates and heat release. These are

$$H_2 + F \xrightarrow{k_1} HF + H, \quad \Delta Q = -32 \text{ kcal mol}^{-1}, \quad k_1 = 2.6 \times 10^{12} T^{0.5} \exp\left(\frac{-610}{RT}\right), \quad (1)$$

$$H + F_2 \xrightarrow{k_2} HF + F, \quad \Delta Q = -98 \text{ kcal mol}^{-1}, \quad k_2 = 3 \times 10^{9} T^{1.5} \exp\left(\frac{-1680}{RT}\right), \quad (2)$$

where k is given in $\text{cm}^3\,\text{mol}^{-1}\,\text{s}^{-1}$, T in K, and R is the universal gas constant in $\text{cal mol}^{-1}\,\text{K}^{-1}$. These are the so-called cold and hot reactions respectively. The cold reaction, which carries 25 % of the total heat release, is faster than the hot reaction by about an order of magnitude at 300 K ($k_1 \approx 1.6 \times 10^{13}$, $k_2 \approx 9.5 \times 10^{11}$). These values are quoted from Cohen & Bott (1982).

Examination of the explosion limits of fluorine–hydrogen mixtures (see Chen, Daugherty & Fyfe 1975; Gmelin 1980) shows that, for the conditions of this experiment, the H_2–F_2 mixture is in a stable region. Thus, it becomes crucial that there be some means to ensure the presence of F *atoms* in order for the the k_1, k_2 reactions to proceed rapidly. The technique used consisted of introducing a small amount of nitric oxide in the hydrogen reactant vessel in such a way that it was uniformly mixed with the hydrogen charge before a run. The nitric oxide reaction proceeds as follows:

$$NO + F_2 \xrightarrow{k_3} NOF + F, \quad \Delta Q = -18 \text{ kcal mol}^{-1}, \quad k_3 = 4.2 \times 10^{11} \exp\left(\frac{-1150}{T}\right) \quad (3)$$

(Baulch *et al.* 1981), while the reverse rate is considered to be negligible (Rapp & Johnston 1960). There is, however, an additional reaction, which scavenges the atomic fluorine and limits the nitric oxide concentration, namely

$$F+NO+M \xrightarrow{k_4} NOF+M, \quad \Delta Q = -57 \text{ kcal mol}^{-1}, \quad k_4 \approx 3\times10^{16} \text{ cm}^6 \text{ mol}^{-2} \text{ s}^{-1} \tag{4}$$

(Baulch *et al.* 1981; Cool, Stephens & Shirley 1970). Consequently the addition of too much NO would itself begin to deplete the available F atoms. For the set of reactions shown here, step (3) is the rate-limiting step. It was determined experimentally that by keeping $[NO][F_2] = 0.03$ [%]^2 the reactions proceed rapidly for $[F_2] = 1$ % molar. In this regard, it is important to note that the addition of 50 % more NO (which increases the overall reaction rate by a proportional amount) showed no significant changes, thus confirming the fact that we had acheived the limit of fast chemistry (see §7).

There are also chain-termination reactions involving three-body collisions of the type

$$\left.\begin{aligned} F+F+M &\xrightarrow{k_5} F_2+M, \\ H+F+M &\xrightarrow{k_6} HF+M, \\ H+H+M &\xrightarrow{k_7} H_2+M, \end{aligned}\right\} \tag{5}$$

where $k_5 \approx 3.2\times10^{14}$ at 300 K, with similar rate constants for the k_6, k_7 reactions (Baulch *et al.* 1981). However, it is easily shown that under the conditions of the present experiments ($[H]/[H_2] \sim [F]/[F_2] \sim [H_2]/[M] \sim [F_2]/[M] \sim 1$ % and $[M] \sim 100$ %) termination reactions are unimportant.

Finally there are energy-transfer reactions of the type

$$HF^*+M \xrightarrow{k_8} HF+M \tag{6}$$

which deactivate the vibrationally excited HF* produced in the hot and cold reactions. For M = N_2, HF, H_2 or F_2, $k_8 \sim 10^9$, 10^{12}, 10^{10} respectively at 300 K. For estimation of rates, if we assume $[HF^*] \sim [HF] \sim 0.5$ %, then comparison of the k_8 rate with the k_3 rate suggests that the deactivation rate is about two orders of magnitude faster than the pumping rate, thus ensuring that the chemical energy of the reaction is rapidly converted into thermal energy.

5. Timescales and flame thickness

The following conditions are typical of the runs performed in this work:

$$\begin{aligned} U_1 &= 22.0 \text{ m s}^{-1}, \quad U_2 = 8.8 \text{ m s}^{-1}, \\ x-x_0 &= 45.7 \text{ cm}, \\ \delta_{\text{vis}} &= 7.4 \text{ cm (visual thickness)}, \\ Re &= \frac{\Delta U \delta_{\text{vis}}}{\nu_{N_2}} = 6.5\times10^4 \quad (\nu_{N_2} \text{ at } 300 \text{ K}), \\ Re_x &= \frac{\Delta U x}{\nu_{N_2}} = 4.0\times10^5. \end{aligned}$$

The large-scale mixing time τ_δ is given by $\tau_\delta \approx \delta_{\rm vis}/\Delta U = 6$ ms, and the small-scale mixing time τ_λ, which is the time to diffuse across the small scale λ, is given by $\tau_\lambda \approx \lambda^2/D \approx \tau_\delta Sc\, Re^{-\frac{1}{2}} = 13$ μs, where D is the mass-diffusion coefficient, and $Sc \equiv \nu/D$ is the Schmidt number. The chemical time is formed from the rate equation (3), and is given by $\tau_c \approx 1/k_3[\mathrm{NO}] \approx 8$ ms using 0.03 % NO at 300 K. The Damkohler number is the ratio of the mixing to the chemical time; thus it is $\tau_\delta/\tau_c \approx 1$ for the large scales, and $\tau_\lambda/\tau_c \approx 4 \times 10^{-3}$ for the small scales. Previously we had estimated the chemical time using a 1 % F_2 concentration with the slower rate k_2. This choice yielded Damkohler numbers of 2×10^3 and 5 for the large and small scales respectively. We now believe that (3), rather than (2), leads to more realistic estimates of the Damkohler number. In this regard, it must be stated it is unclear which numerical value of Damkohler number constitutes fast chemistry. We do note, however, that increasing the Damkohler number by increasing the NO concentration produces no further increase in the amount of product formed. Based on these conditions, this flow can therefore be considered to be a fully developed, turbulent mixing layer in the limit of fast chemistry.

For a diffusion flame that is being strained at a constant rate ϵ, the flame thickness δ_f for large time ($t > 1/\epsilon$) is given by (see Marble & Broadwell 1977) $\delta_f \approx (D/2\epsilon)^{\frac{1}{2}}$. The strain rate can be written as $\epsilon_\delta \approx \Delta U/\delta_{\rm vis}$ for the large scales, and $\epsilon_\lambda \approx \epsilon_\delta Re^{\frac{1}{2}}$ for the small scales. Hence the flame thickness is given by $\delta_f \approx \delta_{\rm vis}(2Sc\, Re)^{-\frac{1}{2}} = 270$ μm for the large scales, and $\delta_f \approx \delta_{\rm vis}(2Sc\, Re^{\frac{3}{2}})^{-\frac{1}{2}} = 17$ μm for the small scales (this small-scale flame thickness is proportional to the Batchelor-scale diffusion thickness). In the Broadwell–Breidenthal model (discussed next), most of the flame elements (flame sheets) are taken to occur at the small scales, so the second expression is probably more representative of the expected flame thickness. The flame sheets are considered to be laminar, strained flames with fast chemistry, occurring throughout the flow, which result in a Burke & Schumann (1928) type thin-flame geometry for which the rate of formation of product is diffusion-limited.

It is worthwhile to note that the cold-wire probe used in the present study has a resolution that is determined by its geometry and response time and is approximately (1.5 mm × 2.5 μm × 5 mm). It is clear that the flame sheet, owing to its very small thickness, as well as the Kolmogorov scale, are beyond the resolution capabilities of the probe.

6. Broadwell–Breidenthal model

This section contains a brief description of the recent Broadwell–Breidenthal (1982) model for mixing and chemical reaction in a turbulent shear layer. It is discussed at this point since some of the results to be presented are interpreted in terms of the model. In this description the term *entrainment* refers to the process by which irrotational fluid is brought into the layer, while the term *mixing* refers to mixing at the molecular level.

This simple model visualizes the mixing process as a sequence of events beginning with the entrainment of pure, irrotational fluid into the layer. The entrained lump of fluid is subsequently broken down into smaller and smaller scales, with rapid increase in the interfacial area, until the smallest scale, the Kolmogorov microscale λ_0, is reached. This entrainment process occurs in a time τ_δ (see §5). Once this occurs, molecular diffusion quickly annihilates any concentration gradients that may exist, and homogenizes the mixed fluid. This is so because the time τ_λ (see §5) to diffuse across the (small) scale λ is given by $\tau_\lambda \approx \tau_\delta Sc\, Re^{-\frac{1}{2}} \ll \tau_\delta$, for $Re \gg 1$.

This leads to an idealization in the model, in which the turbulent mixing layer is decomposed into three types of fluid: (1) unmixed pure reactants, (2) a homogeneous mixture at the entrainment ratio, and (3) fluid in strained laminar diffusion layers (flame sheets) between the free-stream fluids. In the model, the characteristic scale of the homogeneous regions is unspecified, and the flame sheets between the free-stream fluids and the homogeneous mixture are neglected for simplicity. For a reacting flow with fast chemistry, there are known temperatures associated with each of these three fluid types. The pure unmixed fluid is at ambient temperature, since no reaction has yet occurred. The homogeneous mixture attains a uniform temperature determined by the free-stream reactant concentrations and the entrainment ratio, while the flame sheets have a temperature distribution determined by diffusion-flame theory. The mean temperature therefore results from a combination of these three different values. The model also assumes equal diffusivities of all species and unity Lewis number $Le \equiv \kappa/D$ (where κ is the thermal diffusivity and D the mass diffusivity), so that the maximum temperature achieved in the flame sheets will be the adiabatic flame temperature (§1.2).

The relative amount of product in the homogeneous and flame-sheet regions, and the total amount of product, must be determined from experiment. The model does, however, predict that for liquids (e.g. water, $Sc \approx 600$) the product in the flame sheet is negligible and that therefore the total amount of product will be independent of Reynolds number for equivalence ratios larger than the entrainment ratio. The same description of the homogeneous regions applies to gases ($Sc \approx 0.7$), but here the flame-sheet contribution is not negligible and the amount of product there is a function of Reynolds number and equivalence ratio. Thus for similar Reynolds numbers the amount of product generated in a gas is larger than that generated in a liquid by the amount contained in the flame sheets. The model also predicts a dependence upon Reynolds number for the amount of product formed in a gas, but not in a liquid. Thus, strictly speaking, comparisons between gases and liquids, or between gases at different Reynolds numbers, should only be made with this restriction in mind. The dependence upon Reynolds number of the amount of product formed in a gas has been reported by Mungal, Dimotakis & Hermanson (1984). There it was found that the amount of product decreased by 20 % for a factor of 10 increase in Reynolds number (or 6 % per factor of 2). In the comparisons to be made below, these small differences due to Reynolds number will be overlooked.

Broadwell (see Witte *et al.* 1974) has noted that there are two limiting cases for the mixing process. In the first case, if diffusion is slow enough then diffusion across the microscale will be the bottleneck in the sequence of events that culminates in molecular mixing. In this case the mixing is then 'small-scale diffusion-limited'. In the second case, if diffusion is rapid enough, entrainment becomes the slow step in the mixing process. The mixing is then 'entrainment-limited'. Since τ_δ represents the entrainment time and τ_λ represents the time to diffuse across the microscale, then the ratio of these two timescales determines whether the mixing is small-scale diffusion-limited or large-scale entrainment-limited. The ratio is $\mathscr{T} \equiv \tau_\lambda/\tau_\delta \approx Sc/Re^{\frac{1}{2}}$. Thus for $\mathscr{T} \gg 1$ the mixing is limited by the small-scale diffusion, while for $\mathscr{T} \ll 1$ the mixing is large-scale entrainment-limited. For the present high Reynolds number, the flow is therefore entrainment-limited, a condition which should not be confused with that of the (laminar) flame sheets, for which the reactions are diffusion-limited (see Burke & Schumann 1928).

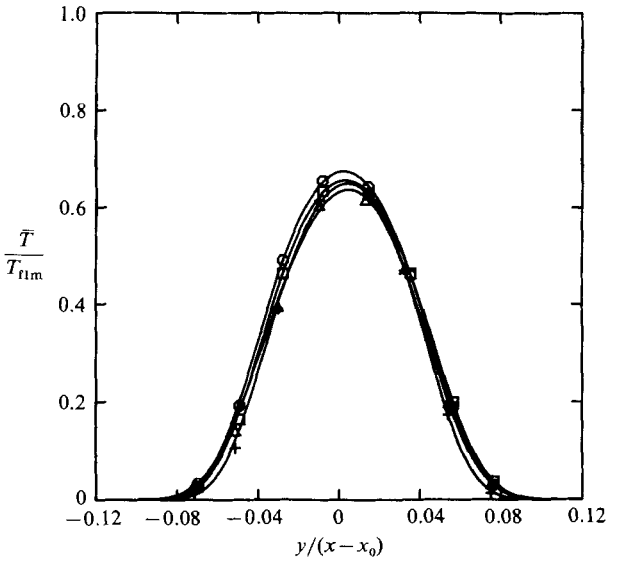

FIGURE 3. Chemistry and ignition; $\phi = 1$. See text for explanation. □, case 1; ○, 2; △, 3; +, 4.

7. Chemistry and ignition

As was noted above, the hydrogen–fluorine reaction is fast and spontaneous for only certain combinations of concentrations of the two species. Hence it is important to determine whether the kinetic rates and the ignition process play a role in results to be described below.

Figure 3 shows the mean-temperature rise (normalized by the adiabatic flame temperature rise) of four runs that were performed to demonstrate that the kinetic rates did not influence the results. (A further discussion of the mean-temperature profile will be provided in §8.) As discussed above, the addition of a small amount of nitric oxide to the hydrogen-carrying stream can be used to ensure rapid ignition. For the majority of runs the product $[F_2][NO]$ was kept at $0.03[\%]^2$, and the nitric oxide was always carried on the hydrogen side. The four runs are

1. 1.0% F_2 on high-speed side, 1.0% H_2 and 0.03% NO on low-speed side;
2. 1.5% F_2 on high-speed side, 1.5% H_2 and 0.02% NO on low-speed side;
3. 1.0% H_2 and 0.03% NO on high-speed side, 1.0% F_2 on low-speed side;
4. 1.0% H_2 and 0.045% NO on high-speed side, 1.0% F_2 on low-speed side, i.e. increase nitric oxide concentration by 50%.

Nitrogen is used as the diluent gas. Cases 1 and 2 test the chemical kinetic rates. Cases 1 and 3 test the effects of interchanging the sides on which hydrogen and fluorine are carried, while cases 3 and 4 test the sensitivity to nitric oxide.

The fact that the mean-temperature profiles repeat each other to within a few percent, despite significant changes in chemical compositions and, of course, chemical rates supports the claims that: first, chemical kinetic rate effects are not important, and we have achieved the limit of fast chemistry; and, secondly, there was sufficient nitric oxide to effect proper ignition. Later, in figure 12, the present results are compared with those of Wallace (1981), who used nitric oxide and ozone as his

reactants, for which the ignition was truly spontaneous. The fact that the temperature profiles agree quantitatively suggests that there are no ignition or chemical kinetic rate problems.

8. Results for equal-density layer

The runs reported here used 1 % fluorine and 1, 2, 4, 8 % hydrogen, both carried in inert nitrogen. The density ratio $s = \rho_2/\rho_1$ was essentially unity for all runs. With fluorine on the high-speed side and hydrogen on the low-speed side it was possible to obtain equivalence ratios of 1, 2, 4, 8. By interchanging the reactants (fluorine on the low-speed side and hydrogen on the high-speed side) it was possible to achieve equivalence ratios of 1, $\frac{1}{2}$, $\frac{1}{4}$, $\frac{1}{8}$.

Figure 4(*a*) shows the time traces from the eight cold wires at an equivalence ratio of unity (1 % F_2 on the high-speed side, 1 % H_2 on the low-speed side). The adiabatic flame temperature (labelled T_{flm}) for this flow is 93 K above ambient, and the time traces show the instantaneous temperature rise T recorded by each probe as a function of time, normalized by the highest temperature rise of any probe during this time interval (labelled $T_{\max}$). The vertical distance between a consecutive pair of horizontal axes therefore represents $T_{\max}$. The horizontal axis corresponds to a total of 51.2 ms of real time. Flow can be viewed as being from right to left with the high-speed fluid on top. The time axis is greatly compressed in the sense that such a plot would be to geometric scale only if the horizontal distance were about nine times the distance between the high-speed and low-speed probes.

Three important features are noticeable in this plot: (1) the presence of large, hot regions or structures; (2) the presence of cool fluid tongues that extend well into the layer; (3) the near-uniformity of the temperature within the structures. These observations are consistent with the earlier results of Brown & Roshko (1974), Dimotakis & Brown (1976), Konrad (1976), Breidenthal (1978, 1981) and Wallace (1981). Figure 4(*b*) shows consecutive time traces for the same run, and has been shaded to enhance the hot regions. In interpreting the time traces, it is useful to keep in mind the fact that the cold wire probe cannot resolve the Kolmogorov scale, so that a certain amount of local averaging takes place.

Figure 4(*c*) shows the results of averaging the time traces for an entire run. A complete run consists of 24 records (such as figure 4*a*) resulting from a total of 98304 recorded points (12288 per probe), during which time at least 100 structures would have passed the measuring station. The circles indicate the measured average temperature rise at the positions of the eight probes, while the smooth curve is an exponential fit of the type

$$\frac{\bar{T}(\eta)}{T_{\mathrm{flm}}} = \exp\left(c_0 + c_1\,\eta + c_2\,\eta^2 + c_3\,\eta^3 + c_4\,\eta^4\right),$$

where $\bar{T}$ is the local mean temperature rise, $\eta \equiv y/(x-x_0)$, and the point $\eta = 0$ corresponds to the position of the dividing streamline. It is significant that the adiabatic flame temperature is not achieved in the mean at any location, a result previously noted by Wallace (1981). The mean profile is seen to result from a duty cycle, i.e. a given probe spends varying lengths of time, dependent upon its position within the layer, in alternate regions of hot and cool fluid. This results in a lower mean temperature towards the outer edges of the layer and a higher mean temperature within. Figure 4(*c*) shows, in addition, the highest and lowest temperatures recorded by each probe during the course of a run. It is clear that the layer can be quite hot

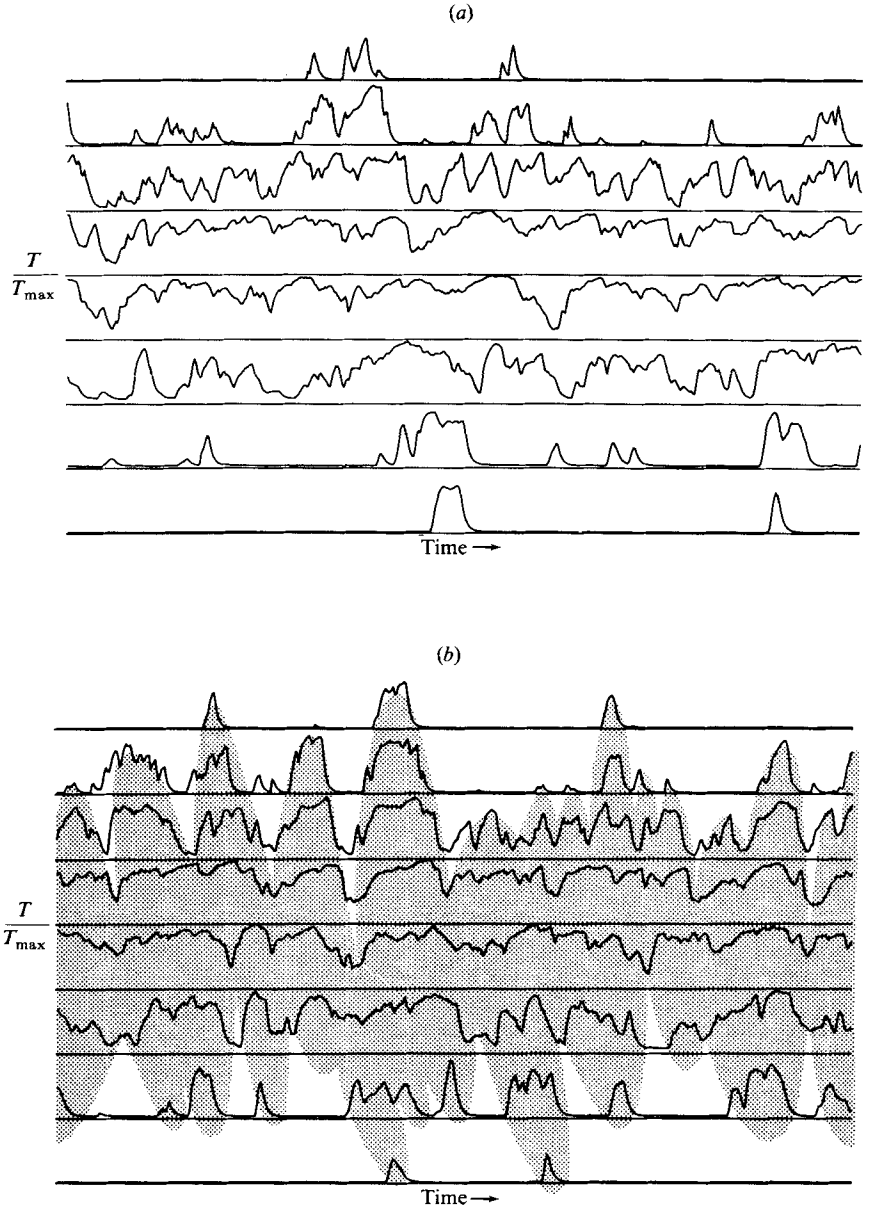

FIGURE 4(a, b). For caption see facing page.

across its entire width (owing to the passage of a large structure) or quite cool across its entire width (owing to the presence of the cool fluid tongues). It must be noted that none of the data shown here are compensated for the thermal lag and conduction error of the wire but, as noted earlier, these errors do not affect the mean-temperature profile. One would expect, in the absence of probe error, that the lowest value measured by each probe would be zero (ambient) temperature, owing to the presence of the irrotational tongues of fluid. One would also expect the highest temperature seen by each probe (for $Le = 1$) to be the adiabatic flame temperature, but as

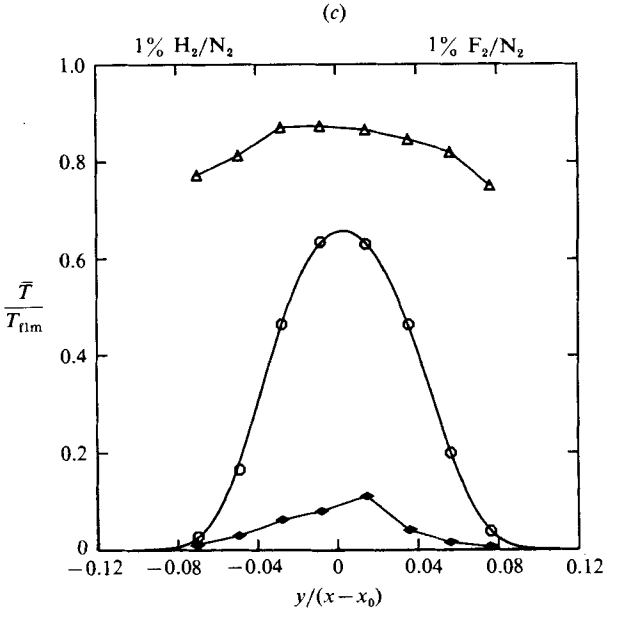

FIGURE 4(*a*,*b*). Temperature *vs.* time trace; $\phi = 1$, $T_{flm} = 93$ K. High-speed fluid on top. Probe positions given by $\eta = 0.076$, 0.057, 0.036, 0.015, −0.008, −0.028, −0.049, −0.070. Time axis = 51.2 ms. (*a*) $T_{max} = 79$ K; (*b*) $T_{max} = 81$ K; (*c*) Mean-temperature profile: $\phi = 1$: ○, mean; △, high; ◆, low.

discussed earlier the cold-wire probes are unable to resolve the region within the flame sheet at which this temperature is attained (Liñan (1974) has shown that, for unequal diffusivities and $Le \neq 1$, the maximum temperature is different from the adiabatic flame temperature, but here we ignore this distinction).

Figures 5(*a*,*b*) show similar results for an equivalence ratio of 4 (1% F_2 on the high-speed side, 4% H_2 on the low-speed side). The adiabatic flame temperature for this flow is 149 K above ambient. All of the main features mentioned earlier are apparent for this case, namely large hot structures, cool fluid tongues and near-uniform cores. The mean temperature profile again does not achieve the adiabatic flame temperature on average, and shows a moderate shift towards the lean reactant, in agreement with Wallace (1981). The layer can still be quite hot or quite cool across its entire width, as shown by the high and low plots.

Finally, figures 6(*a*,*b*) show the results for $\phi = \frac{1}{4}$ (1% F_2 on the low-speed side, 4% H_2 on the high-speed side). These represent the identical reactant compositions with those of the $\phi = 4$ run, but for the fact that they are carried on different sides of the layer (i.e. the reactants have been 'flipped'). The adiabatic flame temperature therefore remains at 149 K above ambient. The time traces show the same main features as discussed earlier. The mean-temperature profile is skewed towards the lean reactant, but is observed to be lower than the case $\phi = 4$, despite the fact that the adiabatic flame temperature and the fluid mechanics are the same in both cases. This finding will be discussed later in the context of the Broadwell–Breidenthal model and the probability density function (p.d.f.) of this flow.

These features were observed for many flows, for a range of equivalence ratios from $\frac{1}{8}$ to 8 with the cases discussed above being quite typical examples (further details can be found in Mungal 1983). The mean-temperature profiles for a set of runs of

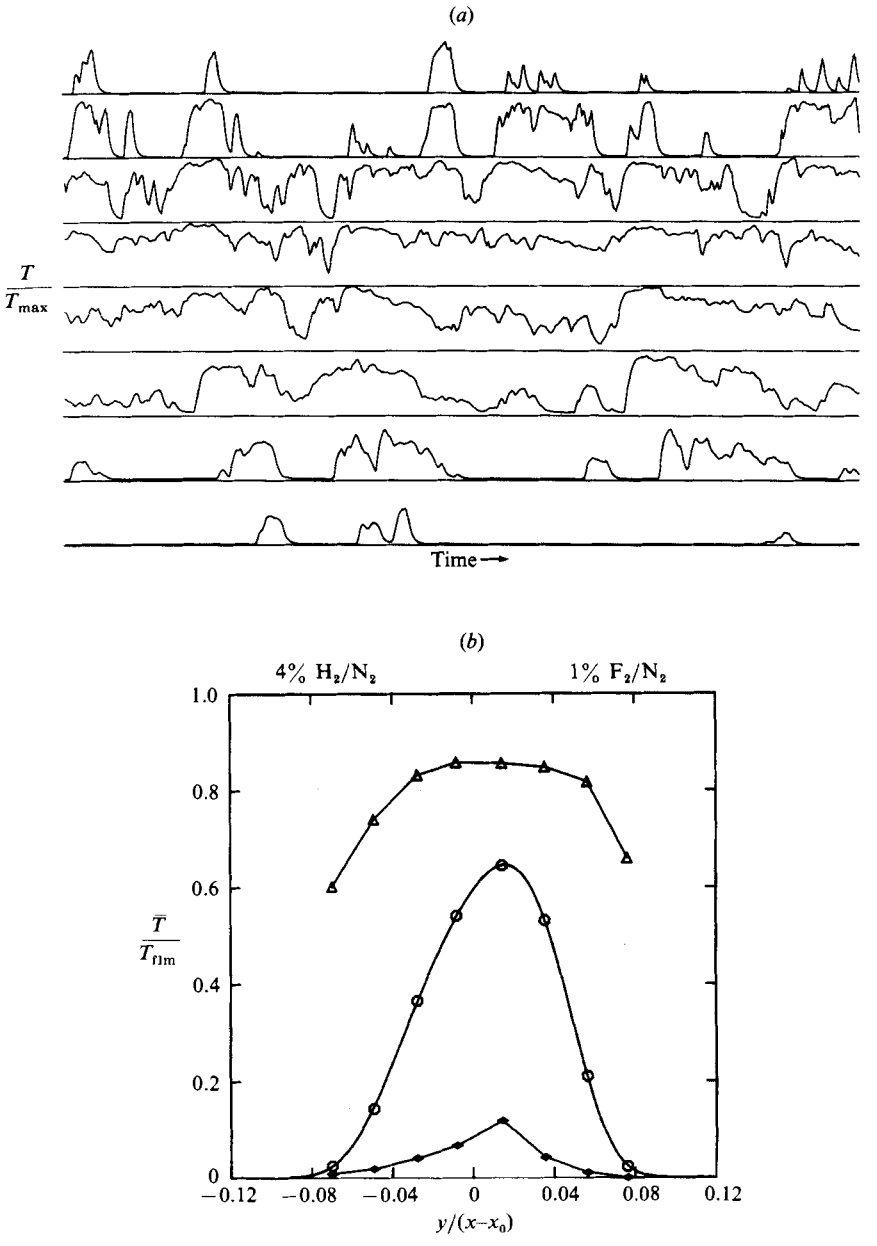

FIGURE 5. (*a*) Temperature *vs.* time trace; $\phi = 4$. $T_{max} = 125$ K. $T_{flm} = 149$ K. High-speed fluid on top. Probe positions same as figure 4. Time axis = 51.2 ms. (*b*) Mean-temperature profile; $\phi = 4$: ○, mean; △, high; ◆, low.

equivalence ratio $\frac{1}{8}$, $\frac{1}{4}$, $\frac{1}{2}$, 1, 2, 4, 8 are shown in figure 7(*a*). Table 1 contains a list of pertinent data for each of these runs. As we noted above for $\phi = 4$, $\frac{1}{4}$, any pair of runs of equivalence ratio ϕ and $1/\phi$ using identical compositions but carried on different sides of the layer (and hence have the same adiabatic flame temperature) produced different mean-temperature profiles. Figure 7(*a*) shows that, with the exception of $\phi = 1$ which repeats to within the experimental error, the results for

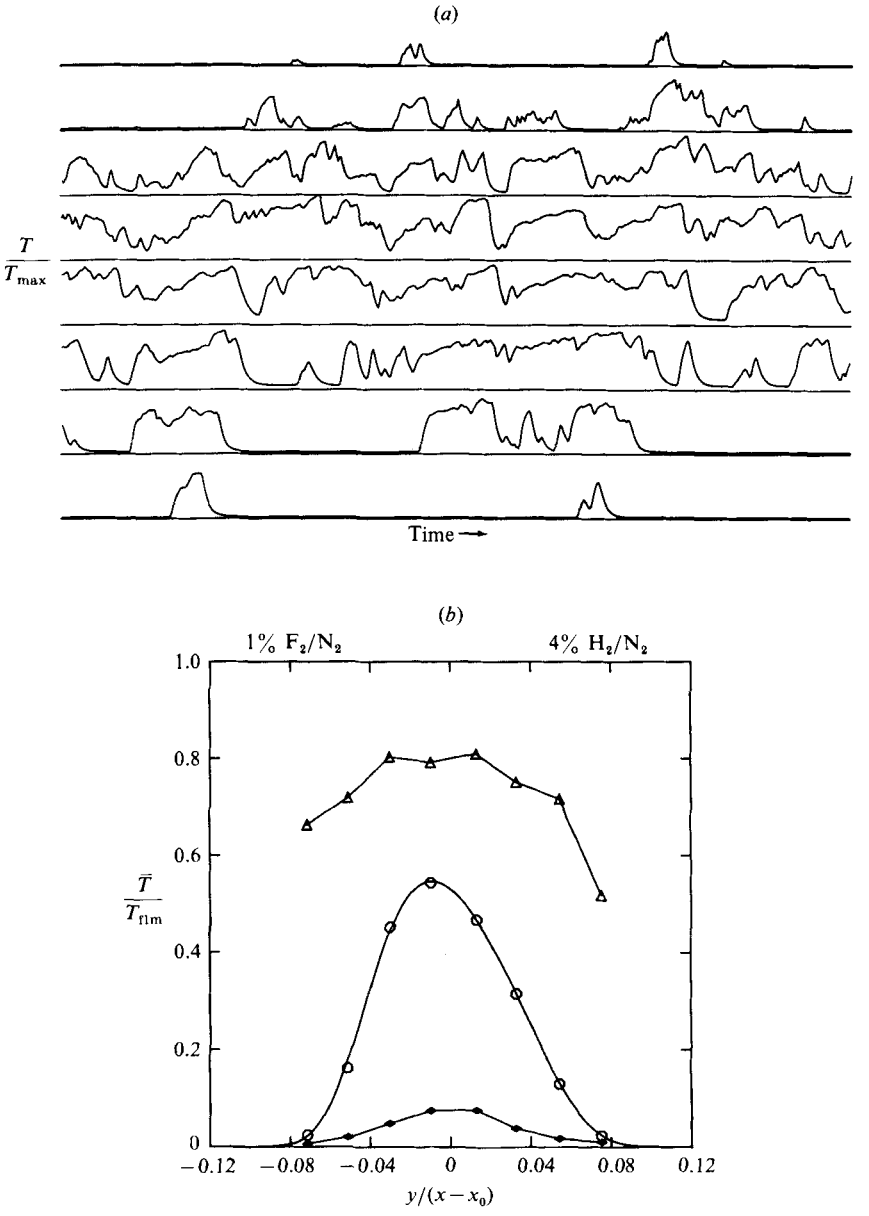

FIGURE 6. (*a*) Temperature *vs.* time trace; $\phi = \frac{1}{4}$, $T_{max} = 121$ K, $T_{flm} = 149$ K. High-speed fluid on top. Probe positions given by $\eta = 0.075, 0.054, 0.033, 0.013, -0.010, -0.030, -0.051, -0.071$. Time axis = 51.2 ms. (*b*) Mean-temperature profile, $\phi = \frac{1}{4}$; ○, mean; △, high; ◆, low.

$\phi = \frac{1}{2}$, 2, $\phi = \frac{1}{4}$, 4, and $\phi = \frac{1}{8}$, 8 are all different. (Pairs of runs such as these which use identical compositions to create equivalence ratios of ϕ and $1/\phi$ will be referred to as flip experiments).

The mean-temperature profiles normalized by the adiabatic flame temperature are shown in figure 7 (*b*). Here it is seen that the maximum mean temperature varies from 0.54 to 0.67 of the adiabatic flame temperature for a range of ϕ from $\frac{1}{8}$ to 8, but is not monotonic with ϕ. The maximum value seems to occur somewhere between $\phi = 1$

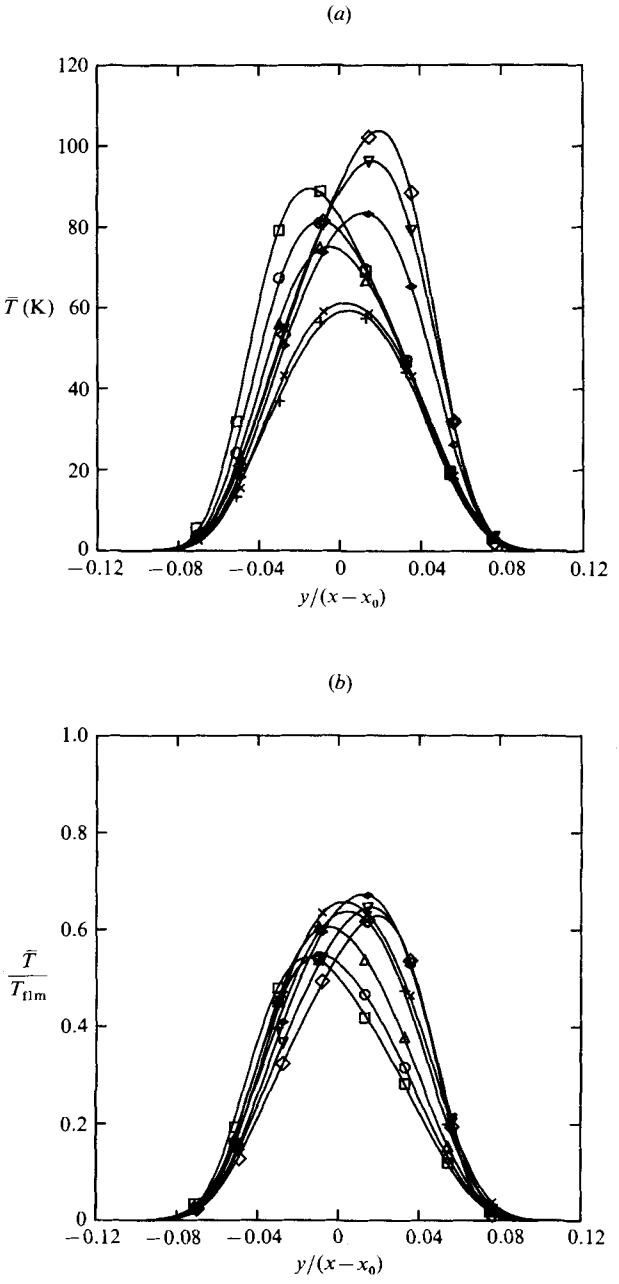

FIGURE 7. Mean-temperature profiles; all ϕ; $s = 1$. Symbols defined in table 1. (*a*) Actual profiles; (*b*) normalized profiles.

and $\phi = 2$. Figures 7(*a*,*b*) also show that the maximum mean temperature shifts by only 25% of the visual width of the layer for a factor of 64 change in equivalence ratio. Such moderate shifts have also been reported earlier by Wallace (1981), and must be related to the p.d.f. of the flow.

Figure 8(*a*) shows the temperature profiles (inferred from figure 7*a*) that would be obtained if the high-speed reactant concentration were held at 1%, with the low-speed

ϕ	Symbol	High speed	Low speed	T_{flm}	$\frac{\overline{T}_{\max}}{\overline{T}_{\mathrm{flm}}}$	Area	$\frac{\delta_1}{x-x_0}$
$\frac{1}{8}$	□	8 % H_2	1 % F_2	165	0.542	0.0442	0.165
$\frac{1}{4}$	○	4 % H_2	1 % F_2	149	0.546	0.0449	0.166
$\frac{1}{2}$	△	2 % H_2	1 % F_2	124	0.605	0.0496	0.168
1	+	1 % H_2	1 % F_2	93	0.638	0.0532	0.170
1	×	1 % F_2	1 % H_2	93	0.657	0.0556	0.168
2	◆	1 % F_2	2 % H_2	124	0.673	0.0552	0.163
4	▽	1 % F_2	4 % H_2	149	0.646	0.0526	0.163
8	◇	1 % F_2	8 % H_2	165	0.628	0.0492	0.159

TABLE 1. Summary of results for figure 7: $T_{\mathrm{flm}} \equiv$ adiabatic flame-temperature rise; $\overline{T}_{\max} \equiv$ maximum value of $\overline{T}$; Area $\equiv \frac{1}{T_{\mathrm{flm}}} \int \overline{T} \mathrm{d}\eta$; $\delta_1 \equiv$ width of layer where $\overline{T} = 1\,\%$ of $\overline{T}_{\max}$

reactant concentration varied from $\frac{1}{8}$ % to 8 %. Similarly figure 8 (*b*) shows the profiles that would be obtained if the low-speed reactant concentration was held at 1 % with the high-speed reactant concentration varied from $\frac{1}{8}$ % to 8 %. If one interprets the area under these curves as being a measure of the amount of product contained in the layer, then it becomes clear that there are two asymptotic values as either the high-speed or low-speed reactant is burned to completion.

Finally, before leaving this section, it must be mentioned that flip experiments have been performed in shear layers in liquids by Koochesfahani, Dimotakis & Broadwell (1983) and Koochesfahani (1984) with equally interesting results.

9. Comparisons

9.1. *Broadwell & Breidenthal*

Flip effects are explained by the Broadwell–Breidenthal theory in a quite straightforward manner. Figure 9 shows a sketch of a typical case for $\phi = \frac{1}{4}$, 4. Use is made of the fact that the entrainment ratio is 1.3 for this particular speed ratio (see Konrad 1976; Brown 1978; Dimotakis 1984). Since the entrainment ratio E may be operationally defined as the ratio of the volume of high-speed fluid to the volume of low-speed fluid molecularly mixed within the layer, the layer contains 30 % more fluid from the high-speed side than from the low-speed side. The sketch shows two typical runs using identical free-stream compositions but carried on different sides of the layer. In case 1 the reactants are 1 % F_2 on the low-speed side and 4 % H_2 on the high-speed side for an equivalence ratio $\phi = \frac{1}{4}$. In case 2 the same reactants are now flipped with 4 % H_2 on the low-speed side and 1 % F_2 on the high-speed side for an equivalence ratio $\phi = 4$. Since the compositions are identical, the adiabatic flame temperature is the same in the two cases and, additionally, the fluid mechanics is unchanged. Thus, in case 1, the lean reactant comes from the low-speed side and consists of 1 part fluorine, which is consumed (burns out) in the large structure to determine the homogeneous temperature. In case 2, the lean reactant now comes from the high-speed side and consists of 1.3 parts fluorine, and it burns out to yield a *higher* homogeneous temperature. In both cases, however, the flame-sheet contribution remains the same, since the amount of product (or contribution to the mean temperature profile) is unaffected by changing the sides on which the chemicals reside.

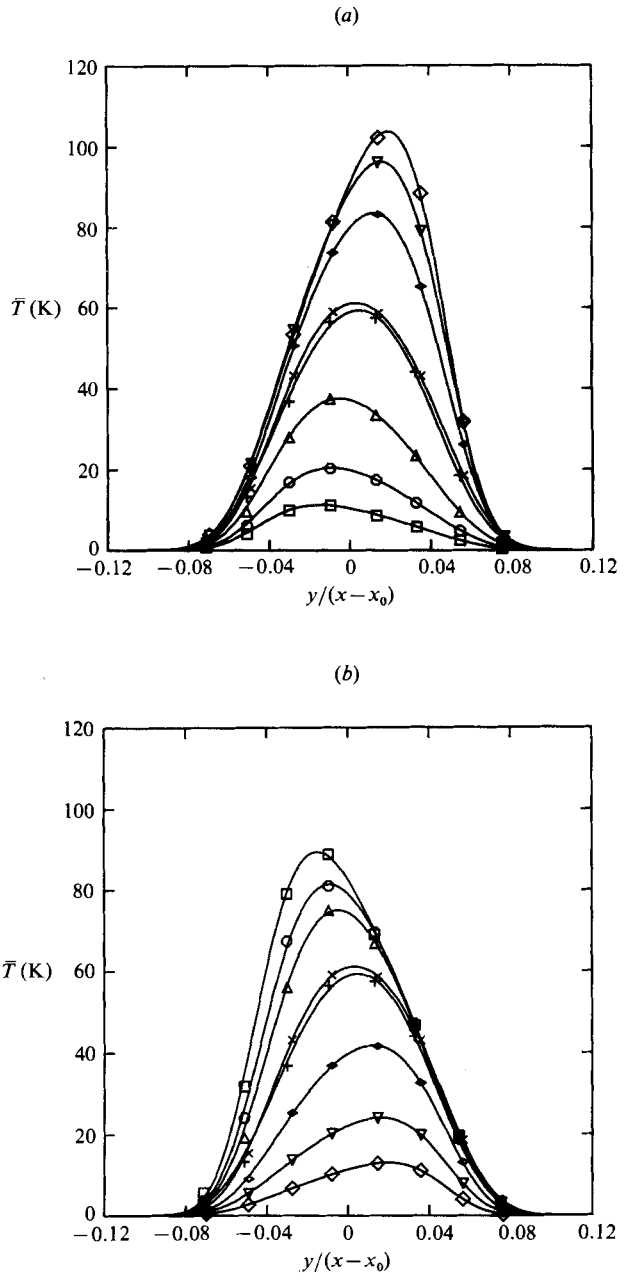

FIGURE 8. Inferred mean-temperature profiles, all ϕ. Symbols same as figure 7. (*a*) High-speed reactant concentration = 1 %; (*b*) low-speed reactant concentration = 1 %.

Thus, case 2 will be hotter than case 1, implying a different mean-temperature profile for the same adiabatic flame temperature and same fluid mechanics.

9.2. *Konrad*

Flip effects can also be derived directly from the earlier measurements of Konrad (1976). As shown in the Appendix, one can generate the mean temperature at each

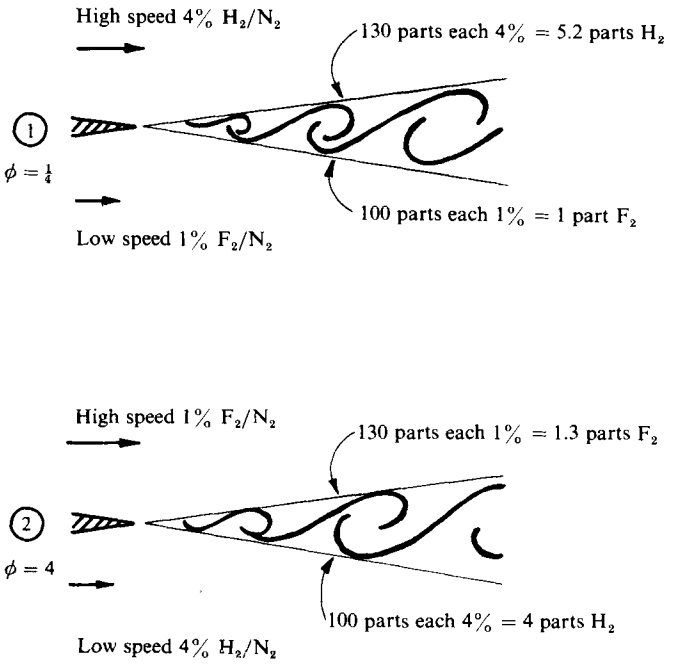

FIGURE 9. Broadwell–Breidenthal view of mixing layer. Case 1, $\phi = \frac{1}{4}$. Case 2, $\phi = 4$.

point across the layer for which the concentration probability density function $p(\xi)$ is known. For the cases $\phi = 4, \frac{1}{4}$ the function $T(\xi)$ will be as discussed in the Appendix. If we now compute the integral

$$\bar{T} = \int_0^1 T(\xi)\, p(\xi)\, \mathrm{d}\xi$$

for each of the Konrad p.d.f.s, then the results for ϕ and $1/\phi$ are different owing to the fact that these p.d.f.s have a peak at approximately $E/(1+E)$, where E is the entrainment ratio (the Konrad p.d.f. is shown and discussed in Broadwell & Breidenthal 1982). In fact, the integrals would only be the same if the set of p.d.f.s were completely symmetric about $\xi = 0.5$ (it is fair to say that, while the Konrad p.d.f.s have been published since 1976, it is only with the advent of the simple Broadwell–Breidenthal model that this implication of the Konrad results was recognized). The mean temperature has been computed using Konrad's p.d.f.s for the cases $\phi = 8,\ 1,\ \frac{1}{8}$ and compared with the experimentally measured results. The comparisons (figures 10*a–c*) show that the concentration probe used by Konrad overpredicted the amount of product by about 40–60 %, depending upon ϕ (Konrad's p.d.f. was measured at a Reynolds number of 4.2×10^4, while the present results are at a Reynolds number of 6.5×10^4, but this difference has been ignored). As mentioned in §1.2, Konrad used the passive-scalar technique, which generally overpredicts the amount of molecular mixing. Koochesfahani & Dimotakis (1984) have measured the p.d.f. of a turbulent mixing layer in water. In spite of the differences in the Schmidt number, their measurements are qualitatively similar to the measurements of Konrad in a gas.

Following Broadwell & Breidenthal (1982), if we idealize the Konrad p.d.f. to be

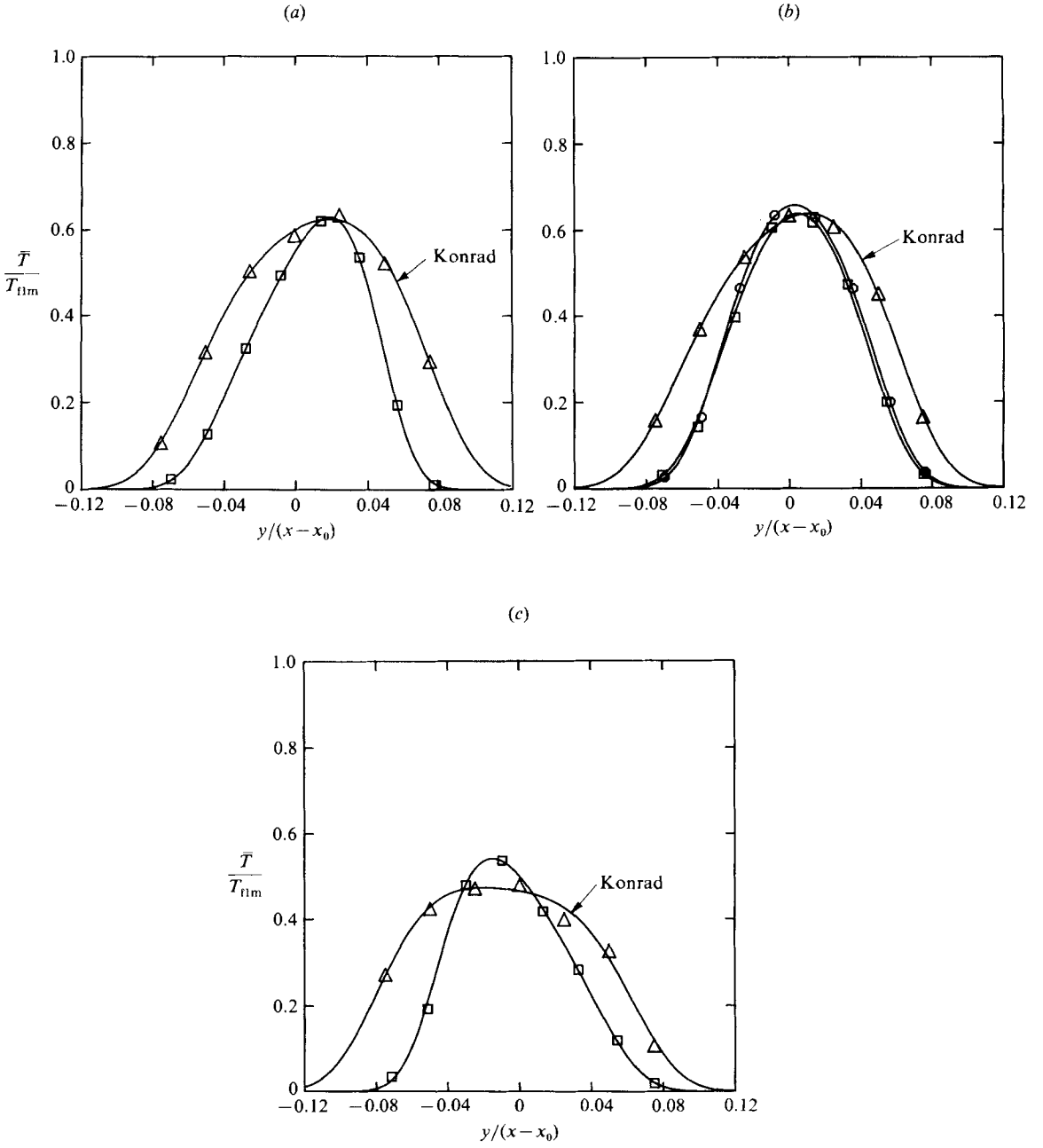

FIGURE 10. Comparison with Konrad; $s = 1$. Experimental curves from figure 7. (*a*) $\phi = 8$; (*b*) 1; (*c*) $\frac{1}{8}$.

a delta function representing unmixed free-stream fluid, together with a dominant value at $E/(1+E)$ representing mixed fluid (figure 11*a*), then the discussion contained in the Appendix suggests that the most-probable values of temperature of the mixed fluid would be approximately the same across the width of the layer. On the other hand, the p.d.f. of Batt (1977) (for a $U_2 = 0$ shear layer) (which has been essentially reproduced by the analyses of Pope (1981) and Kollmann & Janicka (1982)) can be

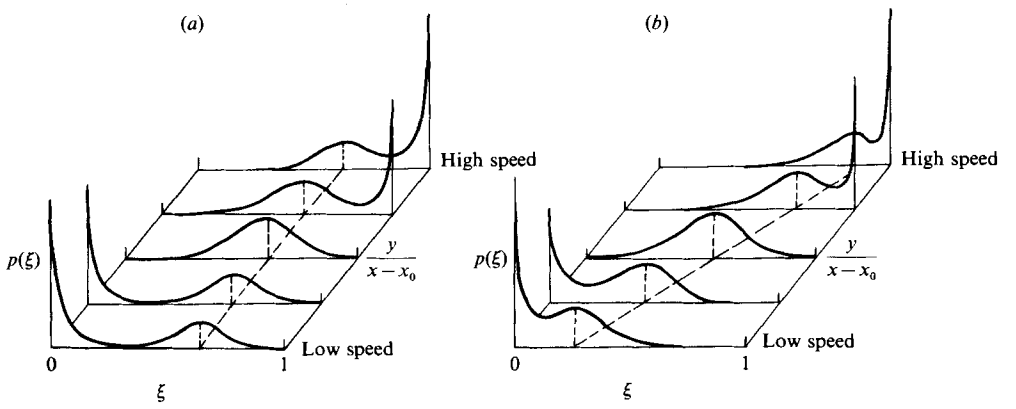

FIGURE 11. Idealized p.d.f. of (*a*) Konrad, (*b*) Batt.

idealized by a free-stream delta function together with a dominant value which *marches* from one edge of the layer to the next (figure 11*b*). Such a p.d.f. would imply most-probable values of temperature that are low at the edges of the layer and high in the middle. The time traces shown above (see figures 4*a*,*b*) suggests most-probable values of the mixed fluid temperature that are the same from one edge of the layer to the next, in closer agreement to the predictions of Konrad than the predictions of Batt. We believe that Batt's resolution, which is about two orders of magnitude worse than Konrad's, is the cause of the discrepancy between the two p.d.f.s.

9.3. *Wallace*

It is also useful to compare the present results with those of Wallace (1981). There are several differences between his experiment and the present work: Wallace used nitric oxide and ozone with a heat release of 47.5 kcal mol^{-1} (*vs.* 130 kcal mol^{-1} for hydrogen–fluorine), the mean temperature was recorded by traversing a fine thermocouple across the layer (*vs.* the present static arrangement of eight cold wires), and most runs were performed at a speed ratio of 0.20. Fortunately, a constant-density (nitrogen–nitrogen) $\phi = 1$ run was performed at a speed ratio of 0.38 using 3 % nitric oxide on the high-speed side and 3 % ozone on the low-speed side. The Reynolds number for this run is about 1.8×10^4 based on velocity difference and visual thickness, which is just past the mixing transition observed by Konrad (1976) and Breidenthal (1978, 1981). This run can be compared with the present 1 % hydrogen–1 % fluorine runs since the heat released is about the same. Since the rate constant for the $NO–O_3$ reaction is approximately 1.0×10^{10} cm^3 mol^{-1} s^{-1} at 300 K (Baulch, Drysdale & Horne 1973), then under these conditions the chemical time for the nitric oxide–ozone reaction is about two orders of magnitude faster than step (3) of the hydrogen–fluorine–nitric oxide system. The comparison is shown in figure 12. Apart from the differences in the location of the dividing streamline, the agreement is quite good, with the amount of product (area under the curves) differing by about 10 %. This agreement is believed to provide an independent check on the present results, despite the differences in Reynolds number and chemical rates.

9.4. *Bernal*

The vortex structure in the turbulent mixing layer has been discussed in detail by Bernal (1981). He suggests an idealized picture in which the streamwise vortices are

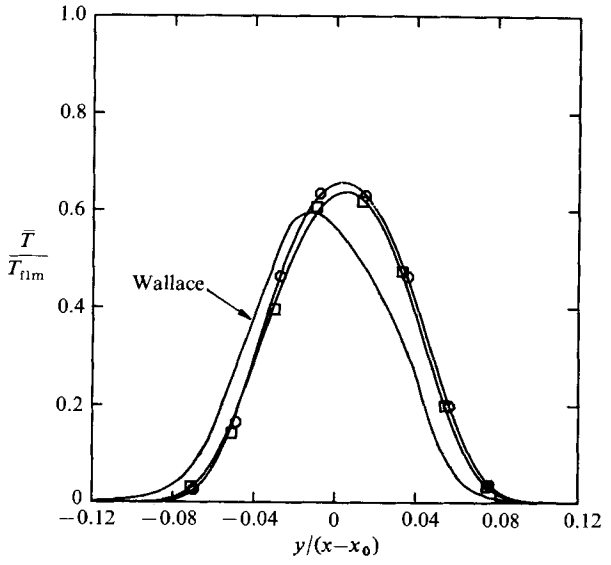

FIGURE 12. Comparison with Wallace; $\phi = 1$. Experimental curves from figure 7.

continuous lines which loop back and forth between adjacent primary vortices and partially wrap around them (the Bernal picture is shown and discussed briefly in Ho & Huerre 1984).

The time traces for $\phi = 8, \frac{1}{8}$, which are reproduced in figures 13(*a*,*b*), show ramps in the streamwise direction, as shown by the shaded areas, and it is useful to interpret this in terms of the Bernal picture. The Broadwell–Breidenthal model suggests that the fluid is homogenized at a single value; however, the Bernal picture would suggest that the effect of the secondary vortices is to add and mix pure free-stream fluid from the outside of the primary vortex towards the inside – this in effect causes a slight gradient in the mixed-fluid composition whereby a given edge of the primary vortex will be biased toward the side of the layer to which it is closest. Thus, for the case $\phi = 8$, the primary vortex will be rich in low-speed reactant, and the leading edge of the structure (early time in the time trace) is expected to be hotter than the trailing edge. The reverse is true for the case $\phi = \frac{1}{8}$, namely the primary vortex will now be rich in high-speed reactant and the trailing edge will be hotter than the leading edge in this case. The shaded areas of figure 13 confirm that this does indeed occur, and lends support to these ideas. Similar gradients are visible in figures 4(*a*) and 5(*a*).

It should also be noted that this interpretation can be applied to the results of Fiedler (1974, 1975) and Rajagopalan & Antonia (1981), who used a temperature rake to study a shear layer in which the high-speed side was slightly heated, and to the measurements of Batt (1977), where the turbulent mixing of both passive and chemically reacting species in a shear layer was investigated. Fiedler finds gradients in the mean mixed concentration in both the normal and streamwise directions that are consistent with the present observations, and similar results are reported by Rajagopalan & Antonia. Batt interprets his results differently, but these gradients are noticeable in his published time traces.

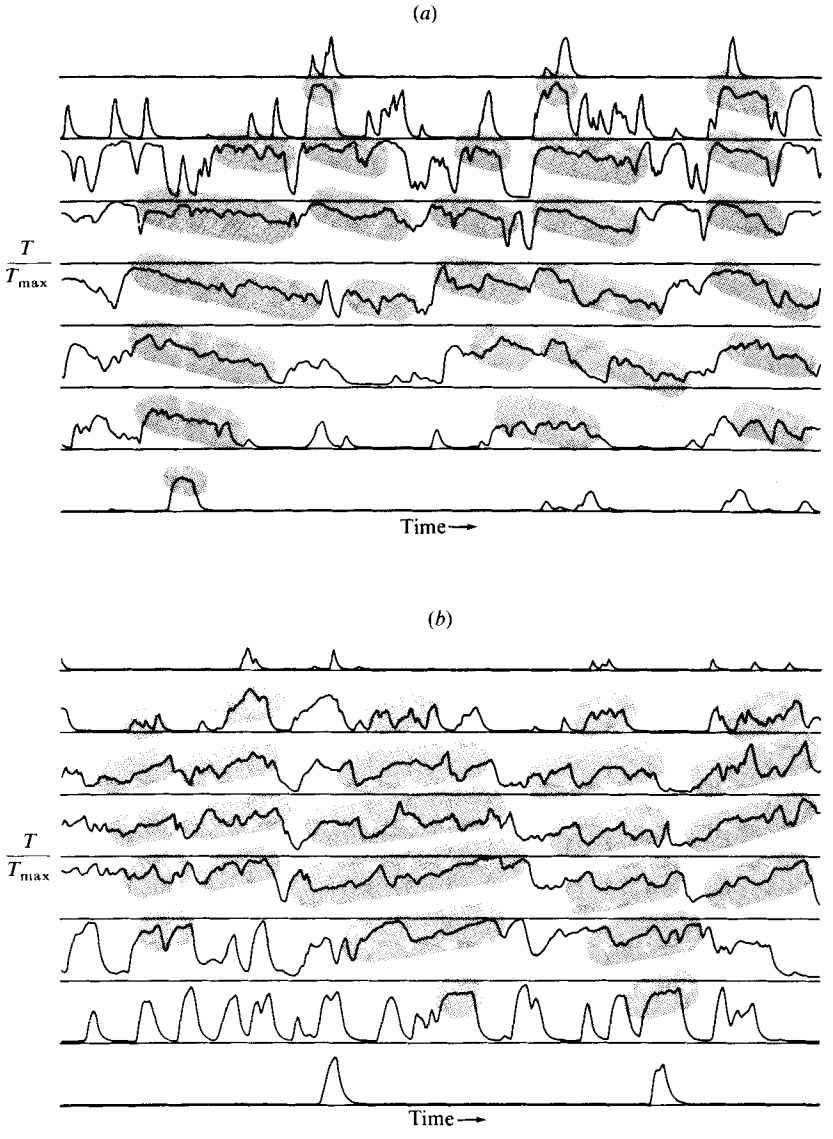

FIGURE 13. Temperature *vs.* time trace: Time axis = 51.2 ms. (*a*) $\phi = 8$, $T_{max} = 137$ K, $T_{film} = 165$ K, probe positions same as figure 4(*a*); (*b*) $\phi = \frac{1}{8}$, $T_{max} = 131$ K, $T_{film} = 165$ K, probe positions same as figure 6(*a*).

10. Comparison with Broadwell–Breidenthal model

The main elements of the Broadwell–Breidenthal model have been discussed earlier (§6). For comparison with the model it was necessary to convert the measured temperature profiles into some measure of product formed. The definition used here is similar to that of Konrad (1976) and Breidenthal (1978, 1981). For a reaction $A + B \rightarrow P$ the product thickness δ_P is defined as

$$\delta_P = \int_{-\infty}^{+\infty} \frac{[c_p(y)]}{c_0} \, dy,$$

i.e. the integral of the concentration of product across the layer is normalized by a selected free-stream concentration c_0. For the present case, since product is proportional to temperature rise, we make use of the measured mean-temperature profile $\overline{T}(y)$, the molar heat capacity C_p of the carrier gas, and the heat release ΔQ per mole of reactant, to obtain

$$\delta_P = \int_{-\infty}^{+\infty} \frac{C_p \overline{T}(y)}{c_0 \Delta Q} \mathrm{d}y,$$

i.e. the temperature rise obtained by burning out the reactant, c_0, is used to normalize the integrated rise across the layer. For later plots the product thickness was made dimensionless with the 1 % thickness δ_1, which is the distance between the points at which the mean-temperature rise is equal to 1 % of the maximum mean-temperature rise. Table 1 lists values of δ_1 for all runs, and a mean value of $\delta_1/(x-x_0) = 0.165$ is used throughout. It should be noted that this value is in good agreement with the Brown & Roshko (1974) formula for the visual thickness:

$$\frac{\delta_{\mathrm{vis}}}{x-x_0} = 0.38 \frac{1-r}{1+r} = 0.163 \quad \text{for} \quad r = 0.4.$$

An important distinction is the choice of the concentration c_0. If this is taken to be the high-speed concentration c_{1_0} then we compute a product thickness δ_{P_1}, while if we choose the low-speed concentration c_{2_0} we compute a different product thickness δ_{P_2}. The corresponding definitions are

$$\delta_{\mathrm{P}_1} = \int_{-\infty}^{+\infty} \frac{C_p \overline{T}(y)}{c_{1_0} \Delta Q} \mathrm{d}y, \quad \delta_{\mathrm{P}_2} = \int_{-\infty}^{+\infty} \frac{C_p \overline{T}(y)}{c_{2_0} \Delta Q} \mathrm{d}y.$$

It is found (see later) that, under the present conditions, for $\phi \gg 1$ the quantity $\delta_{\mathrm{P}_1}/\delta_1$ approaches a limiting value of 0.264, while for $\phi \ll 1$ the limiting value $\delta_{\mathrm{P}_2}/\delta_1$ is 0.237. In general, at the limits, $\delta_{\mathrm{P}_1} > \delta_{\mathrm{P}_2}$ owing to the fact that the layer entrains more fluid from the high-speed side than from the low-speed side. These limits correspond physically to the amount of product formed in the layer as the lean reactant (high-speed or low-speed) is burned to completion.

These two limits can also be related to the p.d.f. for this flow. As discussed in the Appendix, the mean-temperature profile can be computed from

$$\overline{T} = \int_0^1 T(\xi)\, p(\xi)\, \mathrm{d}\xi.$$

For $\phi \to \infty$, $T(\xi) \to \xi$, while, for $\phi \to 0$, $T(\xi) \to 1-\xi$. Thus the δ_{P_1}, δ_{P_2} limits are related to

$$\delta_{\mathrm{P}_1} \sim \int_0^1 \xi\, p(\xi)\, \mathrm{d}\xi, \quad \delta_{\mathrm{P}_2} \sim \int_0^1 (1-\xi)\, p(\xi)\, \mathrm{d}\xi.$$

As discussed earlier (§9) the results are different owing to the fact that the p.d.f. is asymmetric in favour of the high-speed fluid, resulting in the δ_{P_1} limit being larger than the δ_{P_2} limit.

According to the Broadwell–Breidenthal model, the total amount of product contained in the layer is split into a homogeneous part and a flame-sheet part. If we represent the fraction f of the total amount of product that resides as flame sheet, then for $\phi = \phi_1 \gg 1$, and a total amount P_1 of product, the amount $f_1 P_1$ will represent the flame-sheet contribution while $(1-f_1) P_1$ will represent the homogeneous contribution. Here the subscript 1 refers to $\phi \gg 1$, since f is a function of ϕ in the model. Hence the total product P_1 is given by

$$P_1 = (1-f_1) P_1 + f_1 P_1 \quad (\phi = \phi_1 \gg 1).$$

If we now consider the opposite limit $\phi = 1/\phi_1 \ll 1$ (i.e. the flip experiment) then the total amount P_2 of product will decrease, since the homogeneous contribution will be reduced by the entrainment ratio E, but the flame-sheet portion will be unchanged. Thus

$$P_2 = (1-f_1)\frac{P_1}{E} + f_1 P_1 \quad \left(\phi = \frac{1}{\phi_1} \ll 1\right).$$

Solving, we find

$$\frac{P_1}{P_2} = \frac{E}{1-f_1+f_1 E} \quad \text{and} \quad f_2 = \frac{f_1 E}{1-f_1+f_1 E},$$

where f_2 represents the (larger) fraction of the total amount of product that resides as flame sheet for $\phi \ll 1$. For comparison with the model, we have chosen $f_1 \approx 0.5$ for $\phi \gg 1$, i.e. equal amounts of product contained in the homogeneous fluid and the flame-sheet fluid, since with this choice of f_1 and $E = 1.3$ we see that P_1 is approximately 12% greater than P_2, in good agreement with the limiting values of the product thickness quoted above. This is to be contrasted with the predictions of the model for a liquid where there is no flame-sheet contribution ($f \approx 0$) and $P_1 = EP_2$, i.e. a 30% greater amount of product (for this particular value of entrainment ratio). It is useful to note that for larger values of E one can expect larger changes in the amount of product formed as a result of flip experiments (see later results for helium–nitrogen). Recall from §6 that, according to the model, the amount of product in a liquid can be obtained by suppressing the flame-sheet portion of the gaseous result. With our choice of $f_1 = 0.5$, the present gas results would imply a liquid result that is smaller than the value of Breidenthal (1978) (the choice $f_1 = 0.2$ would provide best agreement with Breidenthal). However, Koochesfahani (1984) in more recent experiments suggests that the liquid result may even be less than the Breidenthal value.

To make a comparison with the model it was necessary to use the measured value of δ_{P1}/δ_1 at $\phi = \phi_1 \gg 1$ as an input to the model and to use $f_1 = 0.5$ to extrapolate from $\phi = \phi_1$ to predict the value of δ_{P1}/δ_1 for any other value of ϕ. Alternatively, one can match the value of δ_{P2}/δ_1 at $\phi = \phi_2 \ll 1$, select the flame sheet to homogeneous fluid ratio f_2, and extrapolate to any other value of ϕ. Either approach yields the same results, since selecting the values of the product thickness and the flame-sheet fraction at one limit uniquely determines these quantities at any other value of ϕ.

The measured product thickness δ_{P1}/δ_1 has been plotted versus equivalence ratio ϕ in figure 14. This corresponds to the amount of product contained in the curves of figure 8(*a*). The result of Wallace (1981) for $r = 0.38$, $\phi = 1$ (figure 12) at a lower Reynolds number is also shown. For small values of ϕ, the amount of product increases almost linearly with ϕ as the low-speed reactant is burned out by an excess of high-speed reactant. With further increase in ϕ, an asymptotic limit is reached (past $\phi = 6$) where the high-speed reactant is now burned out by an excess of low-speed reactant with little futher increase in the amount of product. These observations are in general agreement with the earlier results of Wallace (1981) at a speed ratio $r = 0.2$. Konrad (1976) has demonstrated that for the parameter $\alpha = E/\phi$ equal to approximately 0.1 there would be little additional product formed, and the present results agree approximately with this prediction.

The line $f_1 = 0.5$ represents the predictions of the model with agreement forced at $\phi = 8$. The sharp corner or kink in the theoretical curve occurs at $\phi = E$, and results from the assumption that the mixed fluid is homogenized at a single entrainment value $E = 1.3$. In fact, as the Konrad p.d.f.s and the present results suggest, there

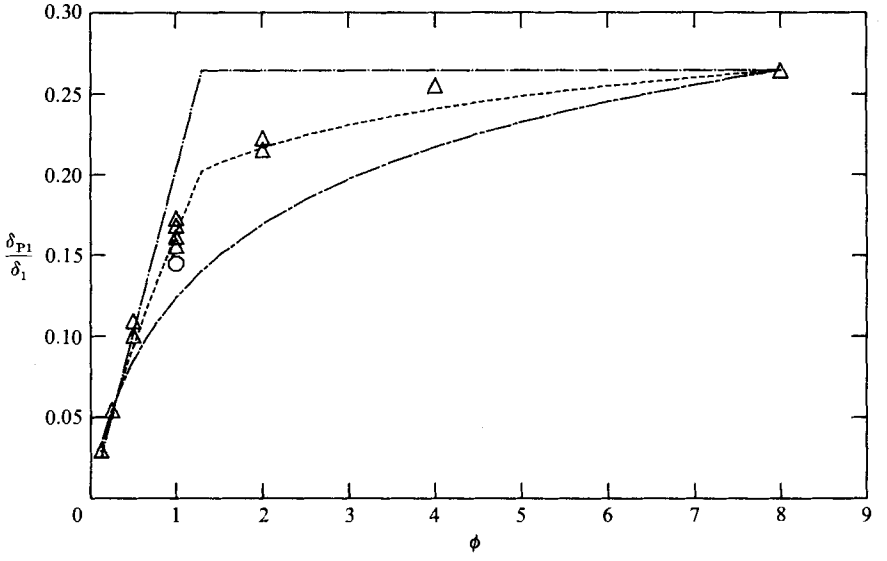

FIGURE 14. Dependence of product thickness on equivalence ratio: △, present results; ○, Wallace; —·—, $f_1 = 0$; – – – – – –, 0.5; ——, 1.

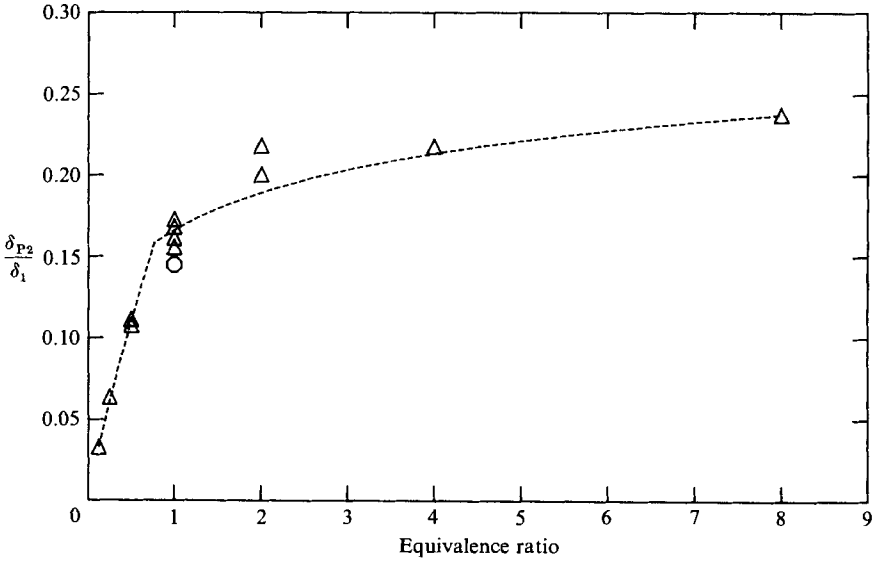

FIGURE 15. Dependence of product thickness on inverse equivalence ratio: △, present results, ○, Wallace. – – – – – –, $f_1 = 0.5$.

is actually a range of mixed-fluid concentrations present, not a single value, and the effect of this would be to round off the sharp corner. Also shown for comparison on this plot are the model predictions for the cases $f_1 = 0$ (no flame-sheet contribution) and $f_1 = 1$ (no homogeneous contribution).

Alternatively, the product thickness δ_{P2}/δ_1 has been plotted versus inverse equivalence ratio ϕ^{-1} in figure 15. This corresponds to the amount of product contained in the curves of figure 8(*b*). The solid line corresponds to the case $f_1 = 0.5$ shown in figure 14.

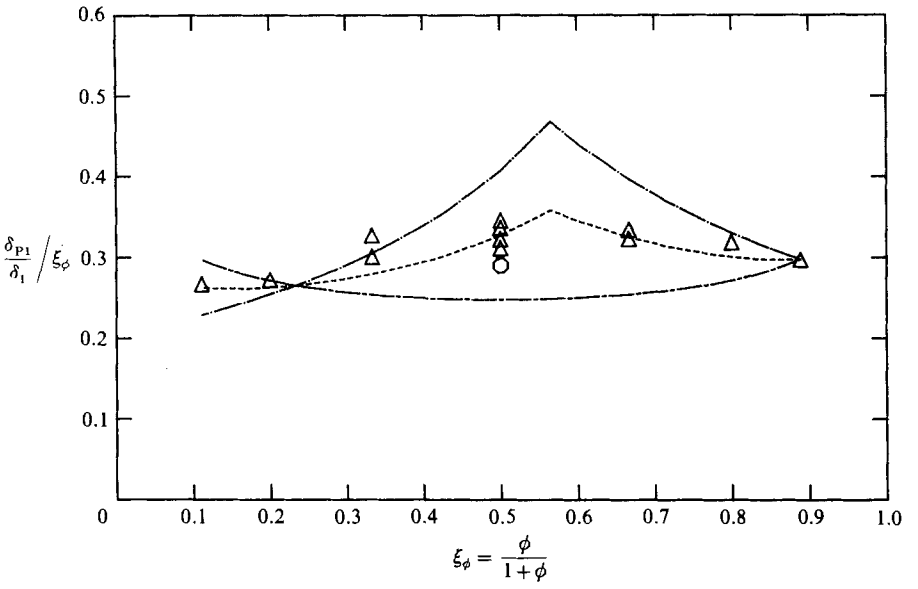

FIGURE 16. Normalized product thickness *vs* normalized equivalence ratio: △, present results; ○, Wallace; —·—, $f_1 = 0$; – – – – –, 0.5; — - —, 1.

In order to remove some of the dependence on ϕ, the results shown in figure 14 have been replotted in figure 16. The horizontal axis is $\xi_\phi = \phi/(1+\phi)$ while the vertical axis is $(\delta_{P1}/\delta_1)/\xi_\phi$. In these coordinates the ordinate lies between 0.25 and 0.35 for the range of ϕ investigated. This curve approaches the δ_{P1} limit for $\xi_\phi \to 1$ and the δ_{P2} limit for $\xi_\phi \to 0$ and again demonstrates the asymmetry in entrainment. The comparisons with the theory with $f_1 = 0, 0.5, 1$ and agreement forced at $\phi = 8$ are also shown.

The result that gases and liquids produce different amounts of product is unexpected from the traditional turbulence viewpoint, since the mass-diffusion coefficient, or the Schmidt number, in non-dimensional form, plays no role. The most obvious question is whether there is independent evidence to support the claim that Schmidt number does indeed play a role. The result was certainly suspected from the earlier work of Konrad (1976) and Breidenthal (1978), but it was not clear if the difference actually existed. Kristmanson & Danckwerts (1961) and Wilson & Danckwerts (1964) performed experiments on a round turbulent jet, both in gas and liquid, to show that there is a Schmidt-number effect on the flame length in the two cases. While we believe that for the two-dimensional mixing layer there is a Schmidt-number effect, Broadwell (1982), using arguments similar to those of the Broadwell–Breidenthal model, has shown that one would expect no change in the flame length of a round turbulent jet as a result of Schmidt-number differences. More recently, Driscoll & Kennedy (1982) have incorporated the Schmidt number into the eddy-breakup model to describe turbulent mixing at high Reynolds number.

11. Results for unequal-density layer

A few runs were performed for a reacting mixing layer consisting of a helium–hydrogen mixture on the high-speed side and a nitrogen–fluorine mixture on the low-speed side. This leads to a density ratio s across the layer of $s = \rho_2/\rho_1 = 7$. Only

small changes in equivalence ratio were made for these runs in an attempt to compare with the equal-density results ($s = 1$) discussed above. It must be noted that there was some uncertainty about the speed ratio for these runs (owing to the difficulty of setting the low dynamic head of the helium stream), but comparison with the Brown–Roshko (1974) growth rates suggest that $r = U_2/U_1 \approx 0.5$. The low-speed velocity was kept at $U_2 = 8.8$ m s^{-1}, and all measurements were taken at $x - x_0 = 45.7$ cm.

The runs performed were

1. $\phi = 1$, 1 % H_2 plus 0.03 % NO in He on high-speed side, 1 % F_2 in N_2 on the low-speed side, $T_{\mathrm{flm}} = 109$ K;
2. $\phi = \frac{1}{2}$, 2 % H_2 plus 0.03 % NO in He on high-speed side, 1 % F_2 in N_2 on the low-speed side, $T_{\mathrm{flm}} = 138$ K;
3. $\phi = 2$, 1 % H_2 plus 0.015 % NO in He on high-speed side, 2 % F_2 in N_2 on the low-speed side, $T_{\mathrm{flm}} = 154$ K.

The mean-temperature profiles are shown in figures 17(a,b). Table 2 contains a summary of pertinent results for these runs. Considering first the $\phi = 1$ case, we note a dramatic change in shape of the mean-temperature profile when compared with the equal-density case discussed above (§7). In addition, the expected 20 % rise in temperature (owing to the lower specific heat of helium) did not occur, a result in agreement with the earlier measurements of Wallace (1981).

Examination of the $\phi = \frac{1}{2}$ case shows only a modest change from the $\phi = 1$ case, but the $\phi = 2$ case produces a significant increase in the mean temperature profile. The increase is due to the large value of the entrainment ratio E for this flow. Konrad (1976) measured $E = 3.5$ with a similarly large value predicted by Dimotakis (1984) (Brown (1974) predicts a somewhat lower value). Thus, if one interprets this flow in terms of a sketch as in figure 9, then compared with the $\phi = 1$ case the addition of excess reactant to the high-speed stream ($\phi = \frac{1}{2}$) produces no change in the homogeneously mixed fluid temperature, whereas the addition of excess reactant to the low-speed stream ($\phi = 2$) produces a doubling of the homogeneously mixed fluid temperature with a net 50 % increase in the amount of product formed. While further work is needed to quantify the differences between the equal-density and unequal-density layers in a systematic way, the results shown here demonstrate that (1) significantly different mean-temperature profiles occur in the two cases; and (2) the much larger entrainment ratio associated with the unequal-density case results in larger changes in the amount of product in flip experiments. Finally, it should be noted that such large asymmetries in the entrainment ratio may have important implications in practical combustor designs.

12. Conclusions

The results presented here suggest that, for the two-dimensional shear layer, mixing and combustion are dominated by the dynamics of the large-scale structures of the flow. It is found that, to first order, the temperature within the large structure is roughly constant. Thus it is possible for the entire width of the layer to be quite hot, owing to the passage of a large structure, or for the layer to be quite cool, owing to the presence of entrained cool irrotational tongues that penetrate deep into the layer. The mean-temperature profile can be considered to be a consequence of a duty cycle whereby a given point in the flow experiences alternating high and low temperatures that average into the local mean. The mean temperature does not attain the adiabatic flame temperature at any location, with the maximum mean temperature

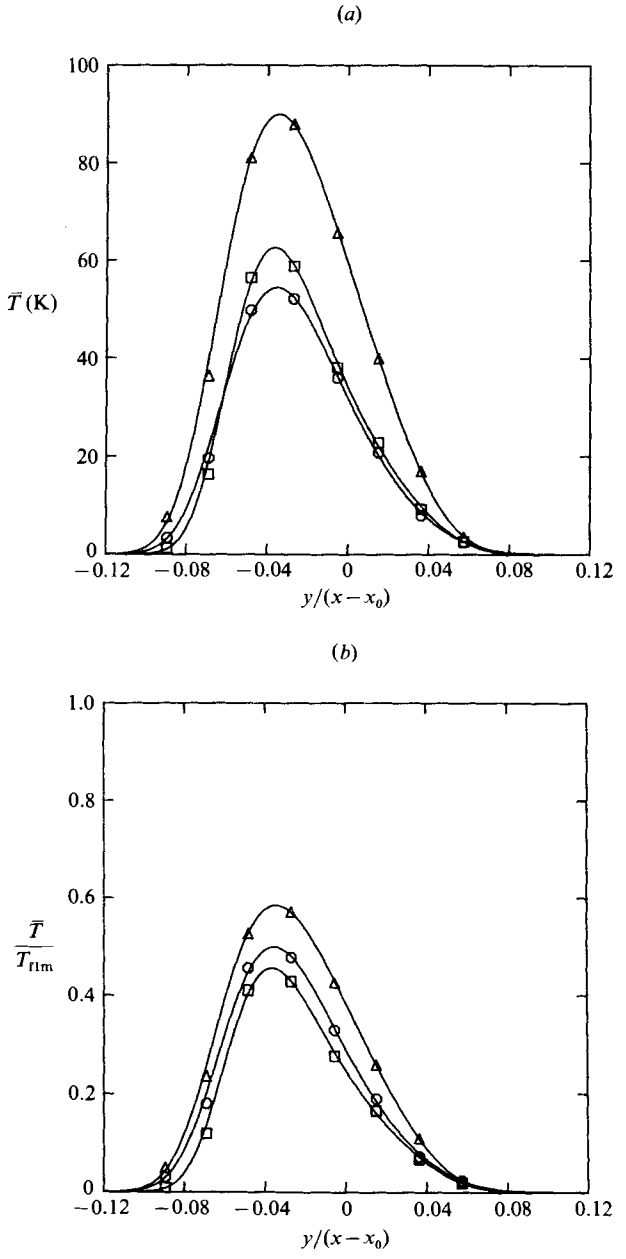

FIGURE 17. Mean-temperature profiles; $s = 7$. Symbols defined in table 2. (*a*) Actual profiles; (*b*) normalized profiles.

ϕ	Symbol	High speed	Low speed	T_{flm}	$\frac{\bar{T}_{\max}}{\bar{T}_{\mathrm{flm}}}$	Area	$\frac{\delta_1}{x-x_0}$
$\frac{1}{2}$	□	2% H_2	1% F_2	138	0.455	0.0320	0.163
1	○	1% H_2	1% F_2	109	0.499	0.0376	0.176
2	△	1% H_2	2% F_2	154	0.584	0.0469	0.173

TABLE 2. Summary of results for figure 17; quantities defined as in table 1

reaching about 50–60 % of this temperature, depending upon equivalence ratio. The shifts in the temperature profiles due to changing equivalence ratio are seen to be slight, with the maximum mean temperature shifting by about 25 % of the visual thickness of the layer for a change of equivalence ratio by a factor of 64. These results are in agreement with the earlier results of Wallace (1981). The mean temperature profiles are compared with calculations based on the Konrad p.d.f.s, and it is found that the concentration probe used by Konrad overpredicted the amount of product formed in the layer by about 40–60 %.

A most interesting result is that the amount of product in the gaseous layer ($Sc \approx 0.7$) is found to be 20 % more than in water ($Sc \approx 600$), as measured by Breidenthal (1978). Results reported by Koochesfahani (1984) indicate that this difference could even be larger. Thus the molecular-diffusion coefficient, or in non-dimensional form the Schmidt number, plays a role in mixing at high Reynolds number. The variation of the amount of product with equivalence ratio has been compared with the predictions of the Broadwell–Breidenthal model and reasonable agreement obtained for a 50 % homogeneous mixture, 50 % flame-sheet decomposition. With this choice, the model also predicts approximately the difference in product in gases and liquids.

Results for a helium–nitrogen layer have been compared with the nitrogen–nitrogen layer. It is found that significantly different mean-temperature profiles occur in the two cases, and larger changes in the amount of product occur for the unequal-density case in flip experiments.

Finally, two other points must be addressed briefly. First, as discussed above, the Broadwell–Breidenthal model predicts a Reynolds-number dependence of the amount of product formed in a gas, and comparisons have been made above with Wallace and Konrad, who worked at Reynolds numbers that are different from that of the present investigation. Based on the experimental results of Mungal *et al.* (1984), it is clear that the comparisons are in general valid. Secondly, it remains unclear how the product is distributed within the large hot regions – 'flame sheets' and 'homogeneous regions' suggested by Broadwell & Breidenthal (1982), 'turbulent part' and 'superlayer part' suggested by Effelsberg & Peters (1983), 'turbules', 'packets', 'folds' and 'eddies' suggested by Spalding (1978) and others. The probe used in the present investigation unfortunately can resolve neither the flame sheets nor the Kolmogorov microscale and must therefore average a volume dictated by its spatial extent and time response.

We would like to acknowledge the significant contributions of B. J. Cantwell and G. L. Brown during the earlier phases of this work, the assistance of J. C. Hermanson and C. E. Frieler in the research reported here, as well as the expert help of Mr Earl Dahl throughout. The many enlightening discussions, critical comments, enthusiastic support and good humour of J. E. Broadwell were especially valuable, and are most appreciated. This work was sponsored by the Air Force Office of Scientific Research contracts F44620–76–C–0046 and F49620–79–C–0159.

Appendix

First consider a turbulent mixing layer with the high-speed side labelled 1 and the low-speed side labelled 2 (for example see figure 1). Consider an infinitesimal sampling volume where we measure (by any possible means) the local instantaneous concentration

$$\xi \equiv \frac{n_1}{n_1 + n_2},$$

where $n_1 \equiv$ number of moles of fluid from side 1 in sampling volume, and $n_2 \equiv$ number of moles of fluid from side 2 in sampling volume. In addition, suppose that n_1 contains n_A moles of dilute reactant A and that similarly n_2 contains n_B moles of dilute reactant B. We define

$$c_{10} \equiv \frac{n_A}{n_1}, \quad c_{20} \equiv \frac{n_B}{n_2}$$

to be the free-stream concentrations of the high-speed and low-speed reactants respectively, and the equivalence ratio

$$\phi \equiv \frac{c_{20}}{c_{10}}.$$

Then the measurement of a concentration ξ implies that n_A moles of A and n_B moles of B are present in the sampling volume. For no reaction they simply coexist, but for a fast reaction (such as burning) the lean reactant will be consumed. Thus for an irreversible reaction of the type

$$1.0\text{A} + 1.0\text{B} \rightarrow 1.0\text{P}$$

the concentration of product is given by

$$[c_P] = \begin{cases} \dfrac{n_A}{n_1+n_2} & (n_A < n_B), \\ \dfrac{n_B}{n_1+n_2} & (n_B < n_A), \end{cases}$$

or

$$[c_P] = \begin{cases} \dfrac{n_A}{n_1}\dfrac{n_1}{n_1+n_2} = c_{10}\xi & (n_A < n_B), \\ \dfrac{n_B}{n_2}\dfrac{n_2}{n_1+n_2} = c_{20}(1-\xi) & (n_B < n_A). \end{cases}$$

The special case $n_A = n_B$ implies stoichiometric conditions, i.e.

$$c_{10}\xi_s = c_{20}(1-\xi_s), \quad \xi_s = \frac{c_{20}}{c_{10}+c_{20}} = \frac{\phi}{1+\phi}.$$

A sketch of $[c_P]$ is shown in figure 18*a*.

By using the heat ΔQ released by the reaction, and the molar specific heat C_p at constant pressure of the inert carrier gas, we see that temperature rise varies directly with $[c_P]$ to obtain

$$T(\xi) = \begin{cases} \dfrac{c_{10}\xi\,\Delta Q}{C_p} & \left(\xi \leqslant \dfrac{\phi}{1+\phi}\right), \\ \dfrac{c_{20}(1-\xi)\,\Delta Q}{C_p} & \left(\xi \geqslant \dfrac{\phi}{1+\phi}\right). \end{cases}$$

This is plotted in figure 18(*b*).

The shape of the curve $T(\xi)$ leads to a double-valuedness, i.e. there are two possible values of ξ (namely ξ_1 and ξ_2 in figure 18*b*) that lead to the same value of T (this corresponds to a given reactant either lean or rich). The only exception to this occurs at ξ_s, when stoichiometry is achieved and the temperature becomes the adiabatic flame temperature, T_f. Figure 19 shows the function $T(\xi)$ for the cases $\phi = \frac{1}{4}, 4$.

Knowing $T(\xi)$ it is possible to use the probability density function $p(\xi)$ for the

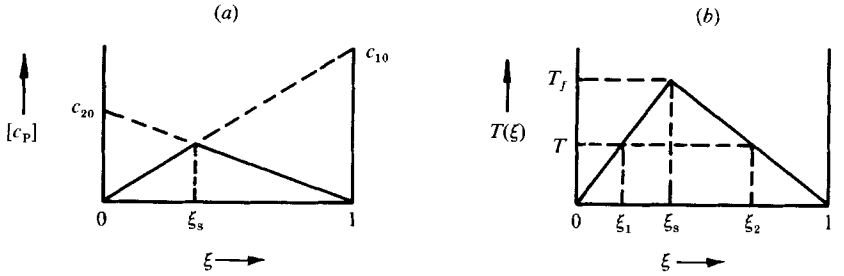

FIGURE 18. (*a*) $[c_p]$ versus ξ. (*b*) $T(\xi)$ versus ξ.

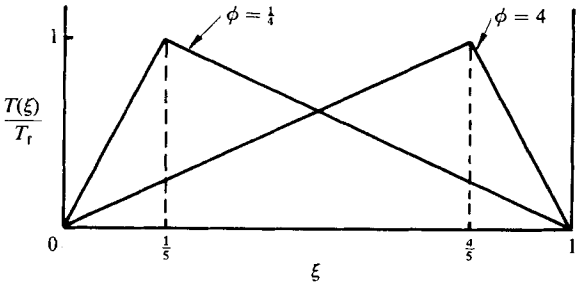

FIGURE 19. $T(\xi)$ versus ξ for $\phi = \frac{1}{4}, 4$.

turbulent mixing layer at a given speed ratio to compute the mean temperature $\bar{T}$ across the layer, since

$$\bar{T} = \int_0^1 T(\xi)\, p(\xi)\, \mathrm{d}\xi.$$

This calculation was performed for each of the seven p.d.f.s measured across the layer by Konrad, using a simple FORTRAN program. The result is discussed in §9.

REFERENCES

BATT, R. G. 1977 Turbulent mixing of passive and chemically reacting species in a low-speed shear layer. *J. Fluid Mech.* **82**, 53–95.

BAULCH, D. L., DRYSDALE, D. D. & HORNE, D. G. 1973 *Evaluated Kinetic Data for High Temperature Reactions*, vol. 2. CRC Press.

BAULCH, D. L., DUXBURY, J., GRANT, S. J. & MONTAGUE, D. C. 1981 Evaluated kinetic data for high temperature reactions, vol. 4. *J. Phys. Chem. Ref. Data* **10**, Suppl. 1.

BERNAL, L. P. 1981 The coherent structure of turbulent mixing layers: I. Similarity of the primary vortex structure. II. Secondary streamwise vortex structure. Ph.D. thesis, Caltech.

BETCHOV, R. 1948 *Proc. Ned. Akad. Wetenshappen* **51**, 721.

BREIDENTHAL, R. E. 1978 A chemically reacting turbulent shear layer. Ph.D. thesis, Caltech.

BREIDENTHAL, R. E. 1981 Structure in turbulent mixing layers and wakes using a chemical reaction. *J. Fluid Mech.* **109**, 1–24.

BROADWELL, J. E. 1982 A model of turbulent diffusion flames and nitric oxide generation part I. *TRW Document* 38515-6001-UT-00.

BROADWELL, J. E. & BREIDENTHAL, R. E. 1982 A simple model of mixing and chemical reaction in a turbulent shear layer. *J. Fluid Mech.* **125**, 397–410.

BROWN, G. L. 1974 The entrainment and large structure in turbulent mixing layers. In *Proc. 5th Australasian Conf. on Hydraul. and Fluid Mech.*, pp. 352–359.

BROWN, G. L. & REBOLLO, M. R. 1972 A small, fast response probe to measure composition of a binary gas mixture. *AIAA J.* **10**, 649–652.

BROWN, G. L. & ROSHKO, A. 1971 The effect of density difference on the turbulent mixing layer. *Turbulent Shear Flows*; *AGARD-CP*-93, 23–1.

BROWN, G. L. & ROSHKO, A. 1974 On density effects and large structure in turbulent mixing layers. *J. Fluid Mech.* **64**, 775–816.

BROWN, J. L. 1978 Heterogeneous turbulent mixing layer investigations utilizing a 2-D 2-color laser Doppler anemometer and a concentration probe. Ph.D. thesis, University of Missouri–Columbia.

BURKE, S. P. & SCHUMANN, T. E. W. 1928 Diffusion flames. *Indust. Engng Chem.* **20**, 998–1006.

CHEN, H., DAUGHERTY, J. D. & FYFE, W. 1975 TA5–H_2/F_2. Flame propagation and repetitively pulsed hydrogen fluoride (HF) chain-reaction laser. *IEEE J. Quantum Electronics* **QE-11**, **8**, 648–653.

CHMIELEWSKI, G. E. 1974 Boundary layer considerations in the design of aerodynamic contractions. *J. Aircraft* **11**, 435–438.

COHEN, N. & BOTT, J. F. 1982 Review of rate data for reactions of interest in HF and DF lasers. *The Aerospace Corp. Rep.* SD-TR-82-86.

COOL, T. A., STEPHENS, R. R. & SHIRLEY, J. A. 1970 HCl, HF, and DF partially inverted cw chemical lasers. *J. Appl. Phys.* **41**, 4038–4050.

DIMOTAKIS, P. E. 1984 Entrainment into a fully developed two-dimensional shear layer. *AIAA*-84-0368.

DIMOTAKIS, P. E. & BROWN, G. L. 1976 The mixing layer at high Reynolds number: large structure dynamics and entrainment. *J. Fluid Mech.* **78**, 535–560.

DRISCOLL, R. J. & KENNEDY, L. A. 1982 A fluid element model for turbulent mixing and combustion. In *Proc. 19th Intl Symp. on Combustion*. The Combustion Institute.

EFFELSBERG, E. & PETERS, N. 1983 A composite model for the conserved scalar PDF. *Combust. Flame* **50**, 351–360.

FIEDLER, H. F. 1974 Transport of heat across a plane turbulent mixing layer. *Adv. Geophy.* **18A**, 93–109.

FIEDLER, H. F. 1975 On turbulent structure and mixing mechanisms in free turbulent shear flows. In *Turbulent Mixing in Nonreactive and Reactive Flows, A Project SQUID Workshop*, pp. 381–410. Plenum.

GANJI, A. T. & SAWYER, R. F. 1980*a* Turbulence, combustion, pollutant, and stability characterization of a premixed, step combustor. *NASA CR* 3230.

GANJI, A. T. & SAWYER, R. F. 1980*b* Experimental study of the flowfield of a two-dimensional premixed turbulent flame. *AIAA J.* **18**, 817–824.

GMELIN 1980 *Handbook of Inorganic Chemistry: F Fluorine Suppl., Vol. 2: The Element*, p. 108. Springer.

HO, C.-M. & HUERRE, P. 1984 Perturbed free shear layers. *Ann. Rev. Fluid Mech.* **16**, 365–425.

KELLER, J. O. & DAILY, J. W. 1983 The effect of large heat release on a two dimensional mixing layer. *AIAA*-83-0472.

KOLLMANN, W. & JANICKA, J. 1982 The probability density function of a passive scalar in turbulent shear flows. *Phys. Fluids* **25**, 1755–1769.

KONRAD, J. H. 1976 An experimental investigation of mixing in two-dimensional turbulent shear flows with application to diffusion-limited chemical reactions. Ph.D. Thesis, Caltech; and *Project SQUID Tech. Rep.* CIT-8-PU.

KOOCHESFAHANI, M. M. 1984 Experiments on turbulent mixing and chemical reactions in a liquid mixing layer. Ph.D. thesis, Caltech.

KOOCHESFAHANI, M. M. & DIMOTAKIS, P. E. 1984 Laser induced fluorescence measurements of concentration in a plane mixing layer. *AIAA*-84-0198.

KOOCHESFAHANI, M. M., DIMOTAKIS, P. E. & BROADWELL, J. E. 1983 Chemically reacting turbulent shear layers. *AIAA*-83-0475.

KRISTMANSON, D. & DANCKWERTS, P. V. 1961 Studies in turbulent mixing – I. Dilution of a jet. *Chem. Engng Sci.* **6**, 267–277.

LIÑAN, A. 1981 Lewis number effects on the structure and extinction of diffusion flames due to strain. In *The Role of Coherent Structures in Modelling Turbulence and Mixing* (ed. J. Jimenez). Lecture Notes in Physics, vol. 136, pp. 333–339. Springer.

MARBLE, F. E. & BROADWELL, J. E. 1977 The coherent flame model for turbulent chemical reactions. *Project SQUID Tech. Rep.* TRW-9-PU.

MUNGAL, M. G. 1983 Experiments on mixing and combustion with low heat release in a turbulent shear flow. Ph.D. thesis, Caltech.

MUNGAL, M. G., DIMOTAKIS, P. E. & BROADWELL, J. E. 1984 Turbulent mixing and combustion in a reacting shear layer. *AIAA J.* **22**, 797–800.

MUNGAL, M. G., DIMOTAKIS, P. E. & HERMANSON, J. C. 1984 Reynolds number effects on mixing and combustion in a reacting shear layer. *AIAA*-84-0371.

PARANTHOEN, P., LECORDIER, J. C. & PETIT, C. 1982*a* Influence of dust contamination of frequency response of wire resistance thermometers. *DISA Info.* **27**, 36–37.

PARANTHOEN, P., PETIT, C. & LECORDIER, J. C. 1982*b* The effect of the thermal prong–wire interaction on the response of a cold wire in gaseous flows (air, argon and helium). *J. Fluid Mech.*, **124**, 457–473.

PITZ, R. W. & DAILY, J. W. 1983 Combustion in a turbulent mixing layer formed at a rearward-facing step. *AIAA J.* **21**, 1565–1570.

POPE, S. B. 1981 A Monte Carlo method for the PDF equations of turbulent reactive flow. *Combust. Sci. Tech.* **25**, 159–174.

RAJAGOPALAN, S. & ANTONIA, R. A. 1981 Properties of the large structure in a slightly heated turbulent mixing layer of a plane jet. *J. Fluid Mech.* **105**, 261–281.

RAPP, D. & JOHNSTON, H. S. 1960 Nitric oxide–fluorine dilute diffusion flame. *J. Chem. Phys.* **33**, 695–699.

SCADRON, M. D. & WARSHAWSKY, I. 1952 Experimental determination ot time constants and Nusselt numbers for bare-wire thermocouples in high-velocity air streams and analytic approximation of conduction and radiation errors. *NACA TN* 2599.

SPALDING, D. B. 1978 A general theory of turbulent combustion. *J. Energy* **2**, 16–23.

TOOR, H. L. 1962 Mass transfer in dilute turbulent and nonturbulent systems with rapid irreversible reactions and equal diffusivities. *AIChE J.* **8**, 70–78.

WALLACE, A. K. 1981 Experimental investigation of the effects of chemical heat release in the reacting turbulent plane shear layer, Ph.D. thesis, The University of Adelaide.

WHITE, F. M. 1974 *Viscous Fluid Flow*, p. 315. McGraw-Hill.

WILSON, R. A. M. & DANCKWERTS, P. V. 1964 Studies in turbulent mixing – II. A hot-air jet. *Chem. Engng Sci.* **19**, 885–895.

WINANT, C. D. & BROWAND, F. R. 1974 Vortex pairing; the mechanism of turbulent mixing-layer growth at moderate Reynolds number. *J. Fluid Mech.* **63**, 417–432.

WITTE, A. B., BROADWELL, J. E., SHACKLEFORD, W. L., CUMMINGS, J. C., TROST, J. E., WHITMAN, A. S., MARBLE, F. E., CRAWFORD, D. R., JACOBS, T. A. 1974 Aerodynamic reactive flow studies of the H_2F_2 laser–II. *Air Forces Weapons Lab., Kirtland Air Force Base, New Mexico*, AFWL-TE-74-78, 33.